Mineral Composition Found in Blue Mud Samples Taken from the Mariana Forearc Aboard IODP Expedition 366

A THESIS SUBMITTED TO
THE GLOBAL ENVIRONMENTAL SCIENCE
UNDERGRADUATE DIVISION IN PARTIAL FULFILLMENT
OF THE REQUIREMENTS FOR THE DEGREE OF

BACHELOR OF SCIENCE

IN

GLOBAL ENVIRONMENTAL SCIENCE

May 2020

By
Marisol Plazas

Thesis Advisors

Patricia Fryer
Przemek Dera
Tayro Acosta-Maeda

We certify that we have read this thesis and that, in our opinion, it is satisfactory in scope and quality as a thesis for the degree of Bachelor of Science in Global Environmental Science.

THESIS ADVISORS

_____

Patricia Fryer
Department of Geology & Geophysics

_____

Przemyslaw Dera
Department of Geology & Geophysics

_____

Tayro Acosta-Maeda
Department of Geology & Geophysics

ACKNOWLEDGMENTS

Patricia Fryer for guidance through the last three years.

The Dera Group, Tayro, and Anupam for advising and instruction.

This research used samples provided by the International Ocean Discovery Program (IODP). Funding for this research provided by USSSP grant 37D(GG009393) via NSF.

ABSTRACT

Large amounts of serpentinite have been reported to be found in the Mariana forearc, forming the largest serpentinite mud volcanoes on earth. International Ocean Discovery Program (IODP) drilling on Yinazao Seamount and Fantangisña Seamounts, two active serpentinite mud volcanoes, recovered samples, and mineral compositions were characterized and compared using X-ray diffraction and Raman spectroscopy.

Samples were sorted into four groups during the study; A, B, C, and D. Groups A, B, and C were dominated by lizardite, a serpentinite mineral. Additional minerals in Group A were andradite, olivine, calcite, garnet, kaolinite, magnetite, brucite, halite, siderite, coalingite, and chrysotile. Additional minerals in Group B were garnet, magnetite, olivine, spinel, and halite. Additional minerals in Group C were oligoclase, olivine, and brucite, magnetite, calcite, halite, goethite, and hydrotalcite, and possibly ferri-clinoholmquistite. Group D was different as it was dominated by feldspars; andesine, oligoclase, labradorite, albite, and clinopyroxene with accessory minerals; tridymite and chloritoid. The minerals found in Group D are commonly found in Mariana lava flows and can likely be found in ash fragments and pelagic sediment. Throughout this study comparisons made between the samples, and thus comparisons of minerals found in the samples indicate that the natural processes of these mud volcanoes have not changed significantly over time except where group D was found. The mineralogy has not changed greatly from early to late eruptions due to the samples being similar at both seamounts as the mud formation processes have not changed greatly between the two sites. Since similar deposits occur worldwide throughout earth's history, serpentinite mud volcano formations could likely be an environment for the origin of life.

TABLE OF CONTENTS

LIST OF TABLES

LIST OF FIGURES

1.0 INTRODUCTION

There are several active serpentinite mud volcanoes on the forearc of Mariana convergent plate margin west of the trench (Fig. 1). Because the Pacific Plate is subducted towards the west beneath the eastern edge of the Philippine Sea Plate, the sea floor west of the Mariana Trench has numerous active serpentinite mud volcanoes, the largest of which has grown to up to three km above the seafloor and reach up to ~50 km in diameter (Fryer et al. 1999). The mudflows form as a result of the release of fluids from the Pacific Plate as subduction carries it down beneath the Mariana forearc (Fryer et al., 1999). The fluids rise through deep-seated faults and interact with the surrounding forearc mantle (Fig. 2), and the composition of the fluids has been shown to change chemically with distance from the trench (Fryer et al., 1999).

The mudflows are produced within deep forearc faults wherein upper mantle rocks are ground up when the fault moves and the resulting ground rock is mobilized and altered chemically to serpentine by rising fluids that are derived from the down going Pacific Plate (Fryer, 1992). When the plate is subducted, it enters higher temperature and pressure conditions within the subduction zone and the subducted Pacific Plate is essentially distilled and releases its fluids, (Mottl, 1992). As the mixture of fluids and ground-up mantle rock rise to the seafloor, they erupt to form the mud volcanoes (Fryer et al., 1999). Also, as this mud rises within the 13 to 19 km deep conduits (Fryer et al., 2018), the fluid interacts with the ground-up mantle rock (mainly olivine and pyroxene) and alters it to serpentine (see reactions below). The resulting mud is less dense than the surrounding mantle rock, helping the mud to rise to form the largest mud volcanoes in the world (Fryer et al., 2019).

Pure Mg-olivine; the major mantle mineral, reacts with water to form serpentine and brucite:

$$2Mg_2SiO_4 + 3H_2O = Mg_3Si_2O_5(OH)_4 + Mg(OH)_2.$$

Most olivine in Mariana forearc mantle rocks contains about 10 mol% Fe. When Fe-olivine reacts with water it oxidizes and forms magnetite and thus liberates hydrogen.

$$3Fe_2SiO_4 + 2H_2O = 2Fe_3O_4 + 3SiO_2(aq) + 2H_2.$$

This process is important for microbial metabolism. Because the fluids are rich in carbonate, they also react with the hydrogen to form methane. The presence of free hydrogen and methane are reasons why serpentinization environments are thought to be likely relevant for the origin of life (Fryer, 2012 and references therein).

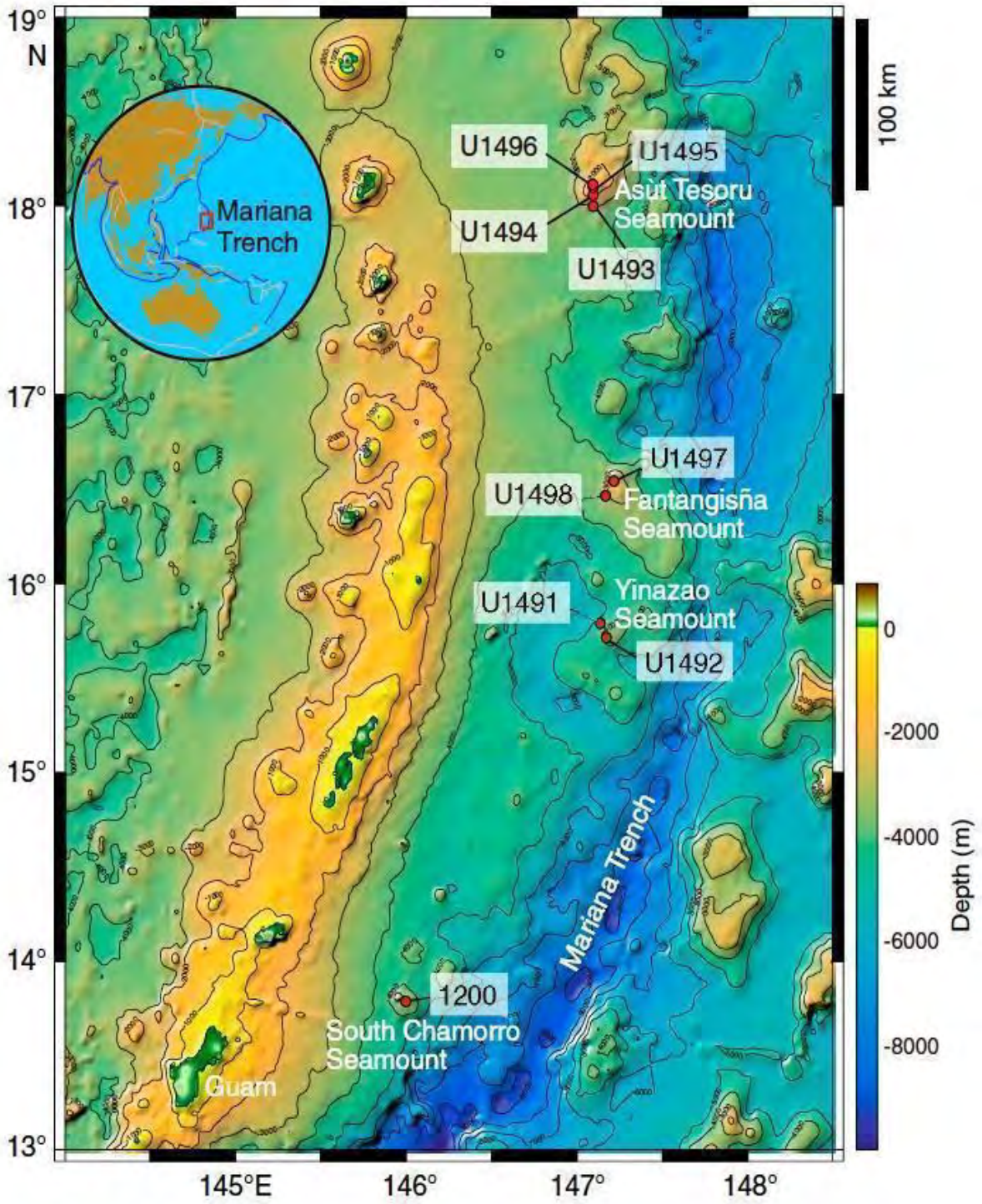

Fig. 1. Map of sampling sites U1491–U1498 on IODP Expedition 366 and site 1200 on South Chamorro Seamount from IODP Expedition 195 (Fryer et al., 2018). Samples for this study were obtained from two of these seamounts; Yinazao (U1492) and Fantangisña (U1498).

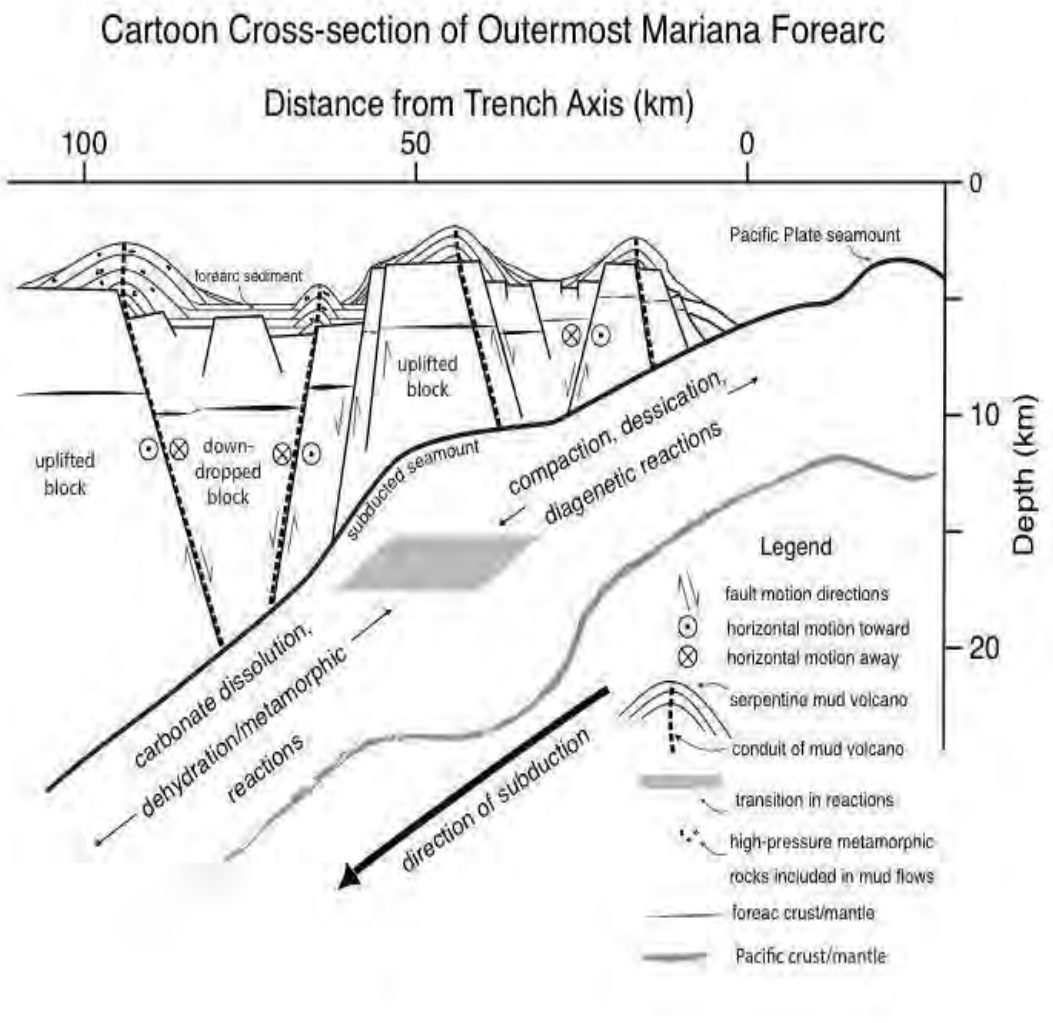

Fig. 2. Subduction of the Pacific tectonic plate beneath the eastern edge of the Mariana forearc (modified after Fryer et al., 1999).

While these processes are well characterized with distance from the trench, a remaining question is whether the processes change with time or location during growth of individual mud volcanoes. The mineralogy of the samples should record any major changes in the processes between the recently erupted mudflows, such as on Yinazao Seamount's summit, as compared to

much older ones, such as on the lower edge of Fantangisña Seamount. Both mud volcanoes were sampled on IODP Expedition 366 to give insight into two key objectives: (a) to "intersect mudflows of variable composition that mantle the flank of each edifice and at Yinazao Seamount, known to be active, recover conduit muds from areas near active springs and;" (b) to "determine variability in the composition of rock clasts in the mudflows" (Fryer et al., 2018) and to contribute mineral data that was not possible to collect during the expedition to aid scientists with their post-cruise research. Initial X-ray diffraction (XRD) analysis of minerals from the core samples was not taken aboard IODP Expedition 366 because the shipboard XRD system was not available during that expedition. The results from this study are the first XRD data to be available for shipboard researchers for comparison with their shore-based research. Knowing the mineralogy of the samples will give a better understanding of the subduction process that takes place to form the mud volcanoes; Yinazao and Fantangisña Seamounts.

We will show that these samples represent material that maintains essentially the same mode of formation involved with serpentine mud volcanism in the Mariana forearc through time. The results provided give a broader insight into the subduction processes within the Mariana forearc over space and time. They will also aid in revealing information about aspects of fluid release from subducting slabs, tectonics of forearc regions (between the trench and arc), and extreme environments that support novel biological communities (Fryer, 1996; Fryer, 2012).

2.0 METHODS

2.1 Sample Collection

The samples used in this study were taken from whole round cores from Yinazao, and Fantangisña Seamounts (Fig. 2). Such cores are collected on IODP expeditions for use in microbial and pore fluid studies. Once they are subsampled aboard the ship the remaining material is available for other analyses. The locations in which each core and thus each sample was gathered in this study are shown in figure 3. The sample names are designated by location (e.g., Site “U1492B”), core number (e.g., “12”), the coring system used (e.g., Half-Length Advanced Piston Corer “F”), and the section cut from the core (e.g., “02”). The last set of numbers in the name of the sample represents the location, in cm, along the 1.5-meter section of the core that the material was taken from. Cores are described by the scientists on the drilling ship and they separate the material into lithologic units (i.e., similar rock or mud types). The units are described in the next section.

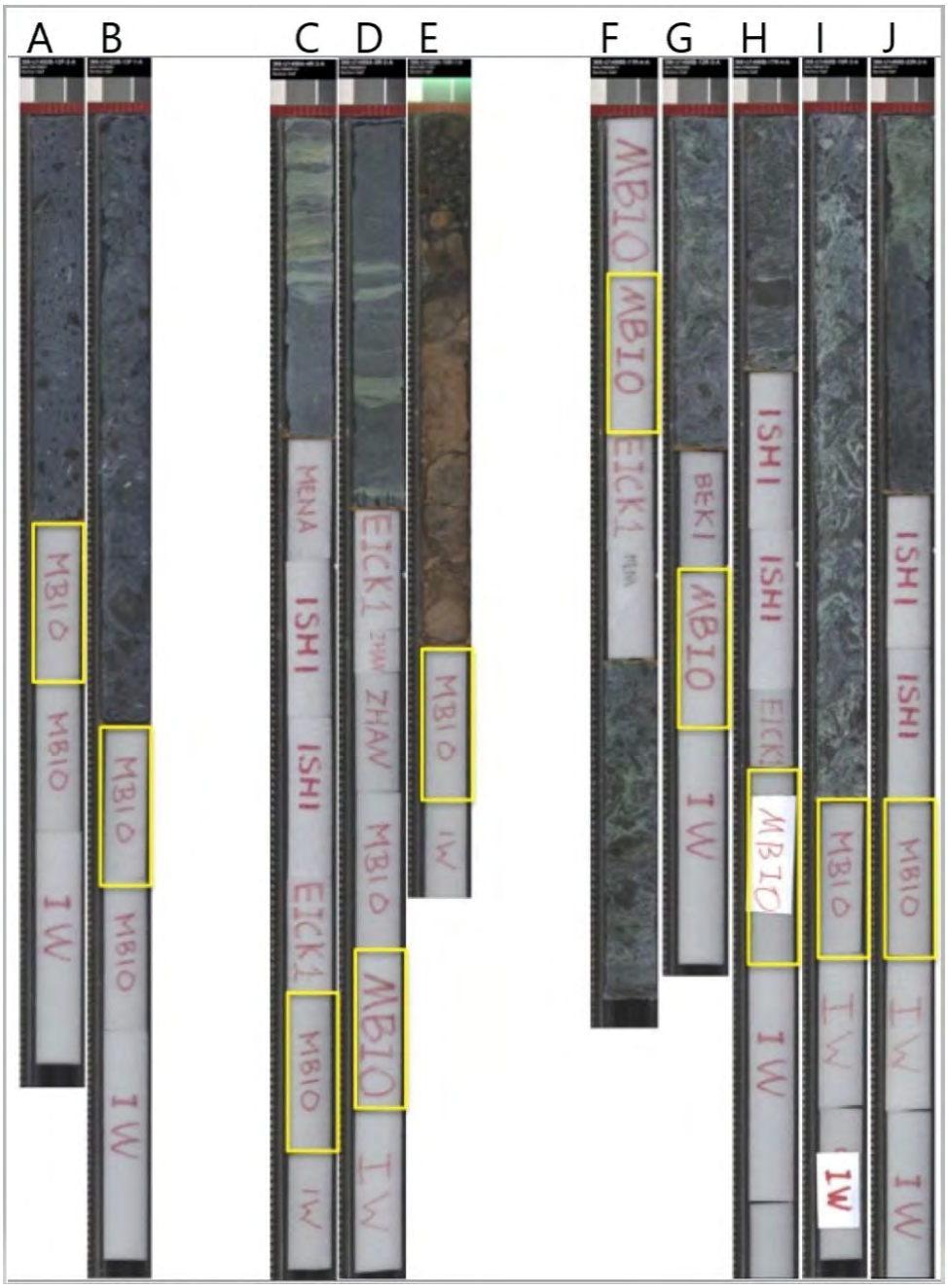

Fig. 3. Photos of the diverse core sections that were sampled for this study. Yellow boxes highlight the areas of these core sections where microbiology whole-round samples were taken that were used for this study. A: U1492B-12F-2 (73-93 cm), B: U1492B-13F-1 (100-120 cm), C: U1498A-5R-2 (104-124 cm) Vial 1, D: U1498A-4R-3 (110-130 cm), E: U1498A-15R-1 (70-90 cm), F: U1498B-11R-4 (20-40 cm) & U1498B-11R-4 (20-40 cm) Fibers, G:U1498B-12R-5 (57-77 cm), H: U1498B-17R-4 (87-107 cm), I: 366 U1498B-19R-3 (90-100 cm), J: U1498B-22R-2 (90-110 cm). Cores A and B were from the Fantangisña Seamount. Cores C, D, E, F, G, H, I and J were gathered from the Yinazao Seamount.

These samples were collected using the following standard coring systems, the advanced piston corer (APC); half-length APC (HLAPC); extended core barrel (XCB); and rotary core barrel (RCB). Samples were individually labeled and cut into 1.5-meter sections for detailed description, sampling, and analyses. Whole-round samples (samples collected from the entire core) were taken immediately after the cores were collected. These whole-round samples were subsampled under sterile conditions and the subsamples preserved for future shore-based analysis, but the outer portions of the whole rounds that remained were made available for use for this thesis. Eleven selected samples gathered from mud flows from Sites on Yinazao and Fantangisña Seamounts are representative of summit and flank cores (respectively).

2.2 Sample Description

2.2.1. Site U1492B

Samples U1492B-12F-02, 73-93 cm, and U1492B-3F-01, 100-120 cm came from the summit of the Yinazao Seamount at 15°42.57′N, 147°10.60′E, in 3666 m of water.

2.2.2. Site U1498A

Samples U1498A-04R-03, 100-130 cm, U1498A-05R-02, 104-124 cm, and U1498A-15R-03, 70-90 cm came from the lower southwest flank Site on Fantangisña Seamount 16°27′N, 147°10′E. Sample U1498A-04R-03, 100-130 cm is from a lithologic unit that is “4.15 m thick and consists of layered serpentinite silt and sand with beds of pelagic sediment, commonly internally graded” (Fryer et al., 2018). Sample U1498A-05R-02, 104-124 cm is from a lithologic unit that is “2.19 m thick and essentially identical to lithologic Subunit IIIA but is separated from it by a 6 m gap” (Fryer et al., 2018). U1498A-15R-03, 70-90 cm is from a lithologic unit “1.65 m thick and consists of dark yellow-brown siltstone and sandstone, much of it broken up by drilling disturbance” (Fryer et al., 2018).

2.2.3. Site U1498B

Samples U1498B-11R-04, 20-40 cm, U1498B-12R-05, 57-77 cm, U1498B-17R-04, 87-107 cm, U1498B-19R-03, 90-110 cm, and U1498B-22R-02, 90-110 cm came from the lower southwest flank of the Fantangisña Seamount, which is located ~3285 m below sea level and ~200m North from Site U1498A, about 700 m higher up the seamount flank. Samples U1498B-11R-04, 20-40 cm, U1498B-12R-05, 57-77 cm, U1498B-17R-04, 87-107 cm, and U1498B-19R-03, 90-110 cm are from a lithologic unit that is ”21.95 m thick and consists of blue-gray serpentinite pebbly mud with lithic clasts” (Fryer et al., 2018). Sample U1498B-22R-02, 90-110 cm is from a lithologic unit “10.45 m thick and consists of bluish-gray to light green serpentinite pebbly mud with lithic rock clasts” (Fryer et al., 2018).

2.3 Laboratory Instruments Used

A Bruker D8 Advance X-Ray Diffractometer and Kaiser 785 nm micro-Raman spectrometry system (Raman) were the two analytical systems used to analyze samples in this study (Fig. 4). XRD analysis was chosen as an “effective method for determining the phase composition (Boughton, 2015) serpentine which has been demonstrated during this study. Raman spectrometry is complementary with XRD as it measures the unique spectrum characteristic of each mineral.

Fig. 4. Venture D8 XRD (Left) and Leica DMLP Raman (Right).

2.3.1 Sample Preparation

Samples were ground in a ceramic mortar and pestle (Fig. 5a) and then sieved through the Frey Scientific Fieldmaster Steel Screen Sieves ranging (Fig. 5b) from 63 to 1000 microns. Each powdered sample was then placed into an XRD sample container (puck) (Fig. 5c) run in a spinning stage with an air scatter slit. XRD data collection was conducted over angular range between 5-80° with a 0.02° step size for roughly one hour.

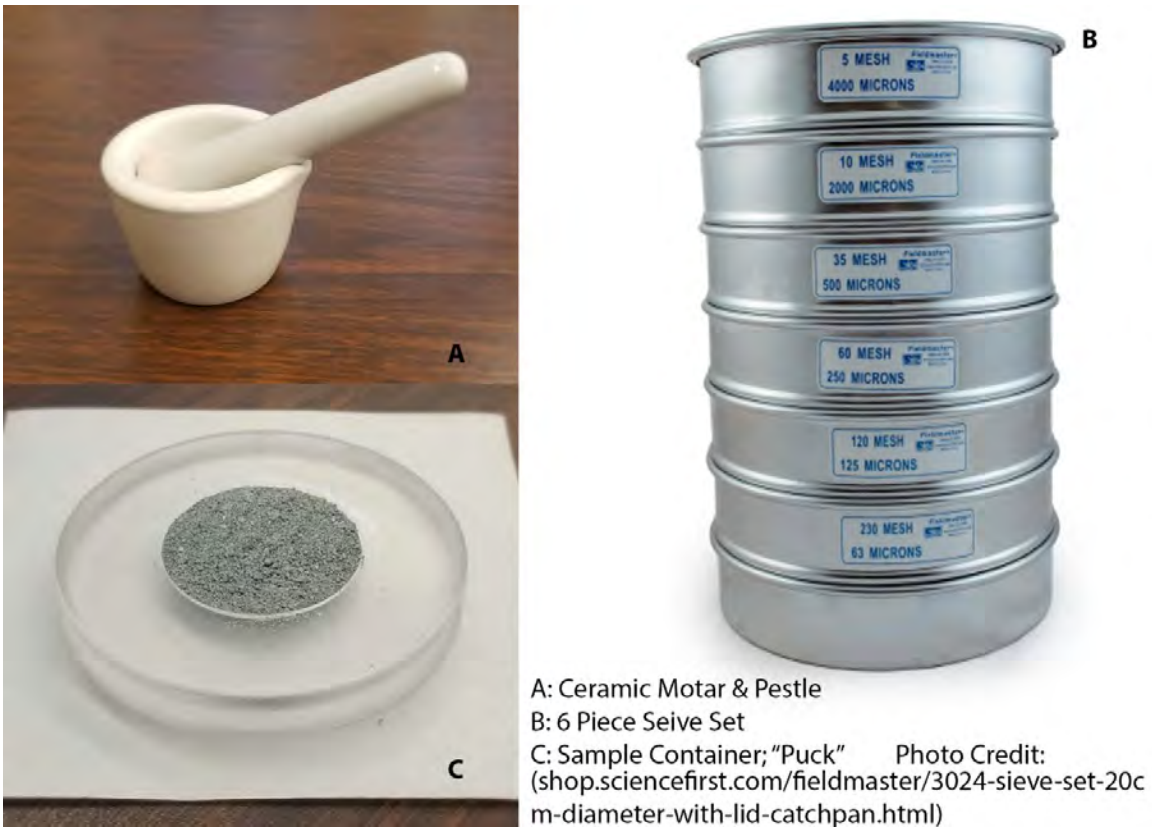

Fig. 5. Sample preparation accessories used to prepare the samples for analysis.

2.3.2 Analysis

During analysis of the XRD spectra, the instrument background was subtracted from each scan in DIFFRAC.EVA (EVA) and was compared to the original scan with the background included, thus verifying peak matches (e.g., Scan1 with background vs Scan1 without background). This was done to compare the similarities of peak positions along the x-axis (2θ values) of the scans. Two compatible computer programs were used: EVA and Topas. EVA was used to identify peak matches to the Crystallography Open Database (COD). The COD database was used to cross-reference past data reports of diffraction patterns of known minerals with EVA's list of observed diffraction peaks via the search/match function. EVA provided a list of ID numbers from the Crystallography Open Database (COD), the ID numbers were used to look up past reports of minerals associated with the ID numbers to check the viability based on

environmental conditions. A list of identified mineral phases was compiled for each scan. To compare the phase compositions of different samples the scans were separated into groups; A (Fig. 3), B (Fig. 4), C (Fig. 5) and D (Fig. 6) by prominent peaks and the location of peak intensity, peak width, and peak positions. Group A (Fig. 6) represented a base reference, as it had the least amount of peaks. This group contains four samples that recovered from the deep flank of the Fantangisña Seamount (U1498), and one sample that was recovered from the recently active Yinazao Seamount (U1492). Yet, the differences in the XRD patterns between these samples were exceedingly small. Group B (Fig) also presented a set of remarkably similar scans. In Group B (Fig. 7) the XRD spectra showed a small shoulder peak on the left side of the major peak at about 2θ =11. Two of the spectra are from the deep flank of Fantangisña Seamount and one is from the Yinazao Seamount. Group C (Fig. 8) had multiple minor new peaks introduced in addition to the group A baseline, which means very minor mineral phases and no peaks at about 2θ=11 such as in Group B. The two spectra in Group C are both found at the Fantangisña seamount. All three of the samples presented a peak at 2θ =11 signified a major similarity between groups A, B, and C. Group D consists of U1498A-15R-01 (70 – 90 cm) as this sample is an outlier. This is because it came from beneath the serpentinite mud flows of Fantangisña Seamount. Distinguishing between different serpentine minerals is difficult, due to low crystallinity and structural defects. Most natural samples available as references are phase mixtures of serpentine polytypes. To identify the type of serpentine phases in our samples, the XRD data were compared with results given in Kohyama (2007, see Fig. 10), which was key in differentiating between chrysotile, lizardite, and antigorite. The four groups are further described in the results section.

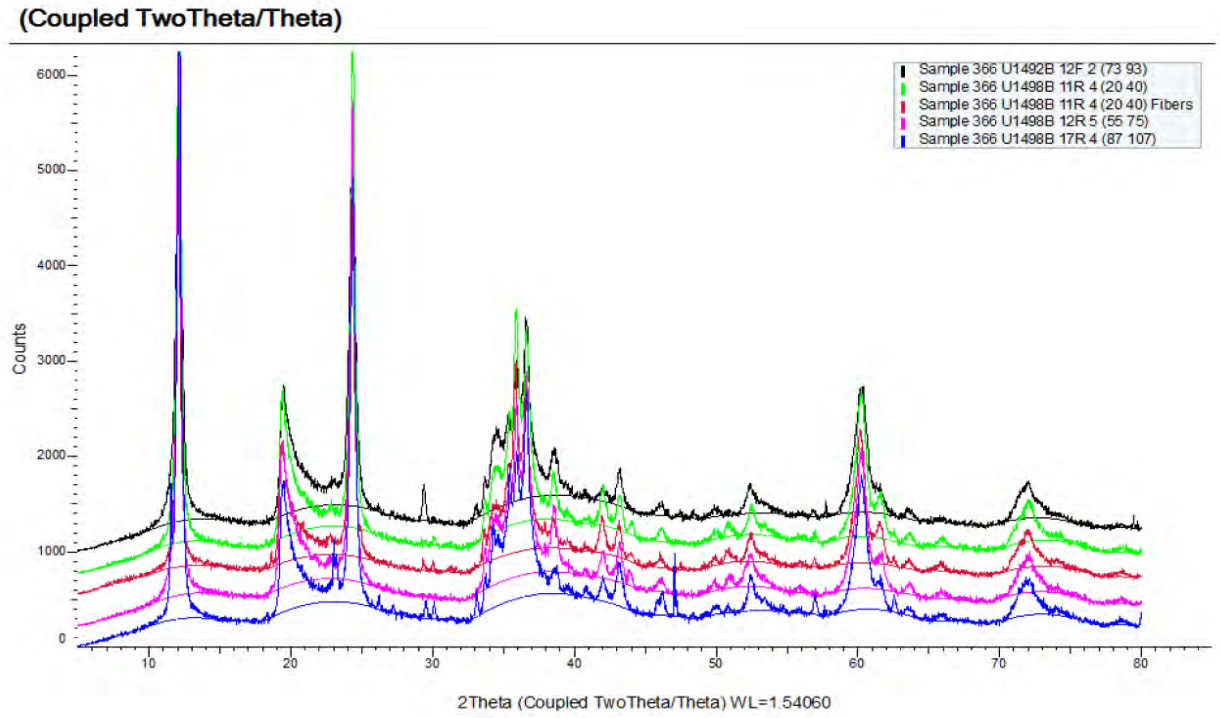

Fig. 6. Group A comprises of Samples U1498B-12R-05 (57 – 77 cm), U1498B-11R-04 (20 – 40 cm) U1498B-11R-04 (20 – 40 cm) Fibers, U1498B-17R-04 (87 - 107 cm) and U1492B-12F-02 (73 – 93 cm) shows strong peaks at 2θ =12, 2θ =19, 2θ =24.5, 2θ =36.5 and 2θ =60.1, the peaks with the most counts identified served as the "base" diffractogram and were the easiest to identify.

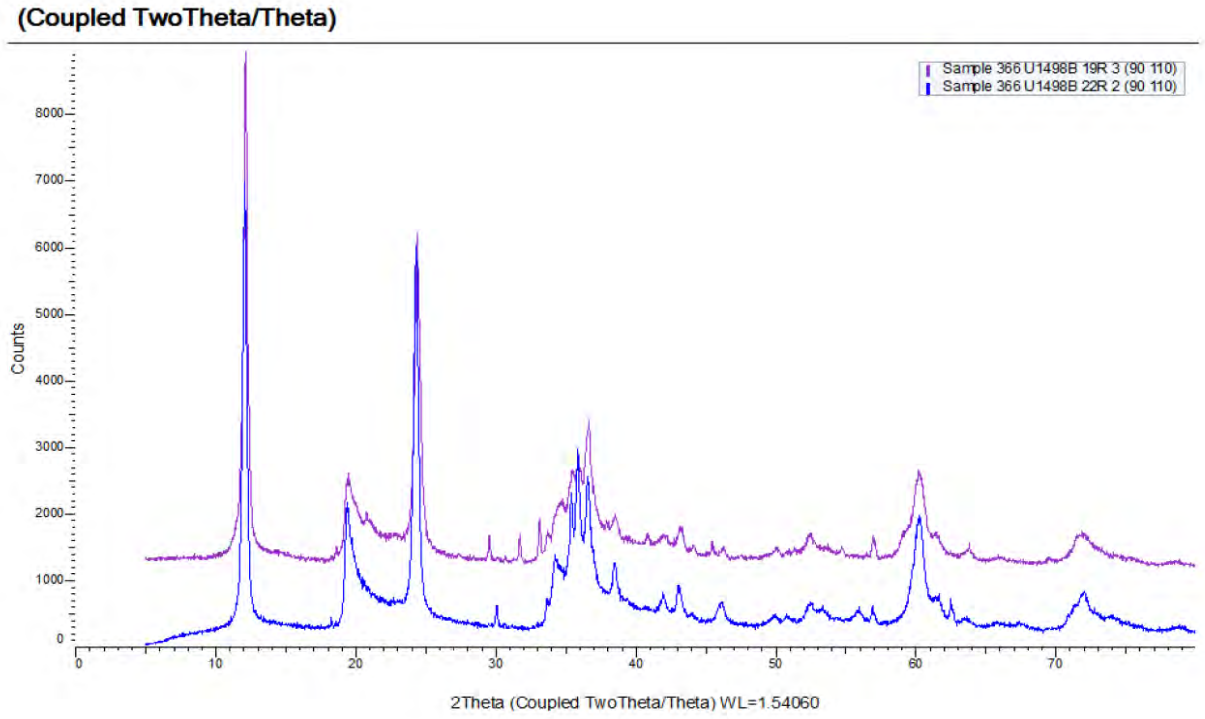

Fig. 7. Group B consists of U1498B-22R-02 (90 – 110 cm) and U1498B-19R-03 (90 -110 cm) to show the similarities between both scans. Similarities identified between the two spectra are at 2θ =30, 2θ =38.5, 2θ =42, 2θ =43, and 2θ =50.

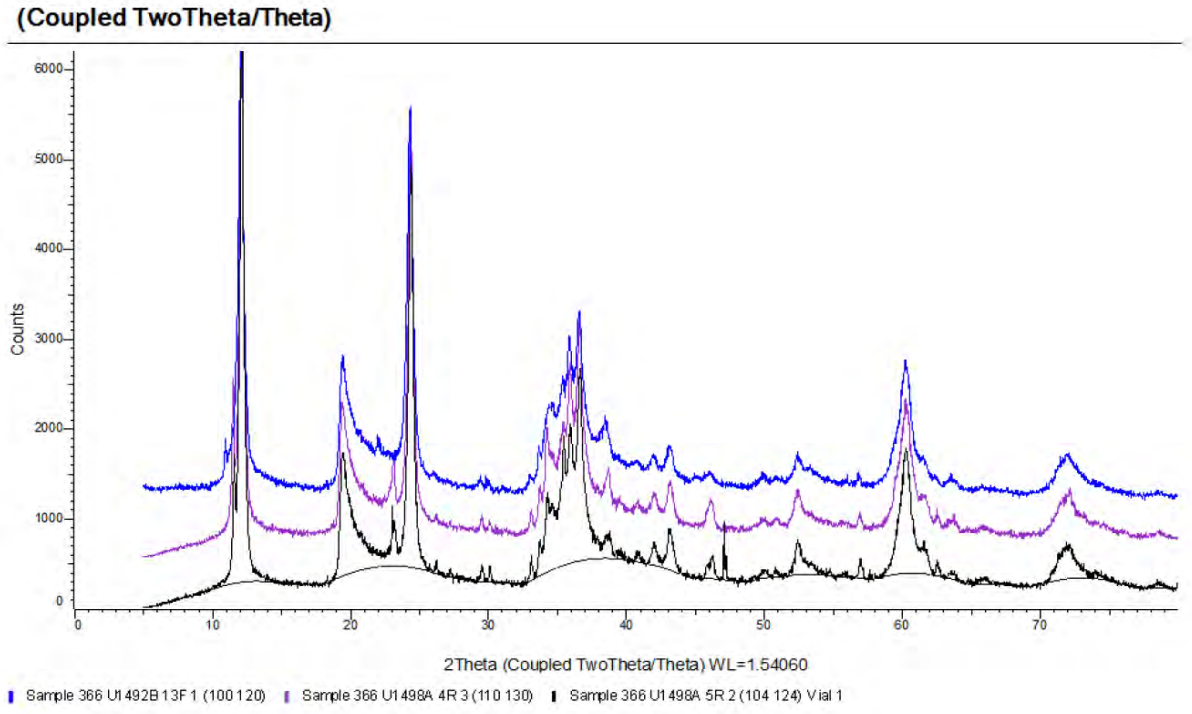

Fig. 8. Group C consists of U1492B-13F-01 (100 -120 cm), U1498A-04R-03 (110 -130 cm), and U1498A-05R-02 (104 – 124 cm) vial 1 to show the similarities between each scan. The major similarity presented is at 2θ =11.

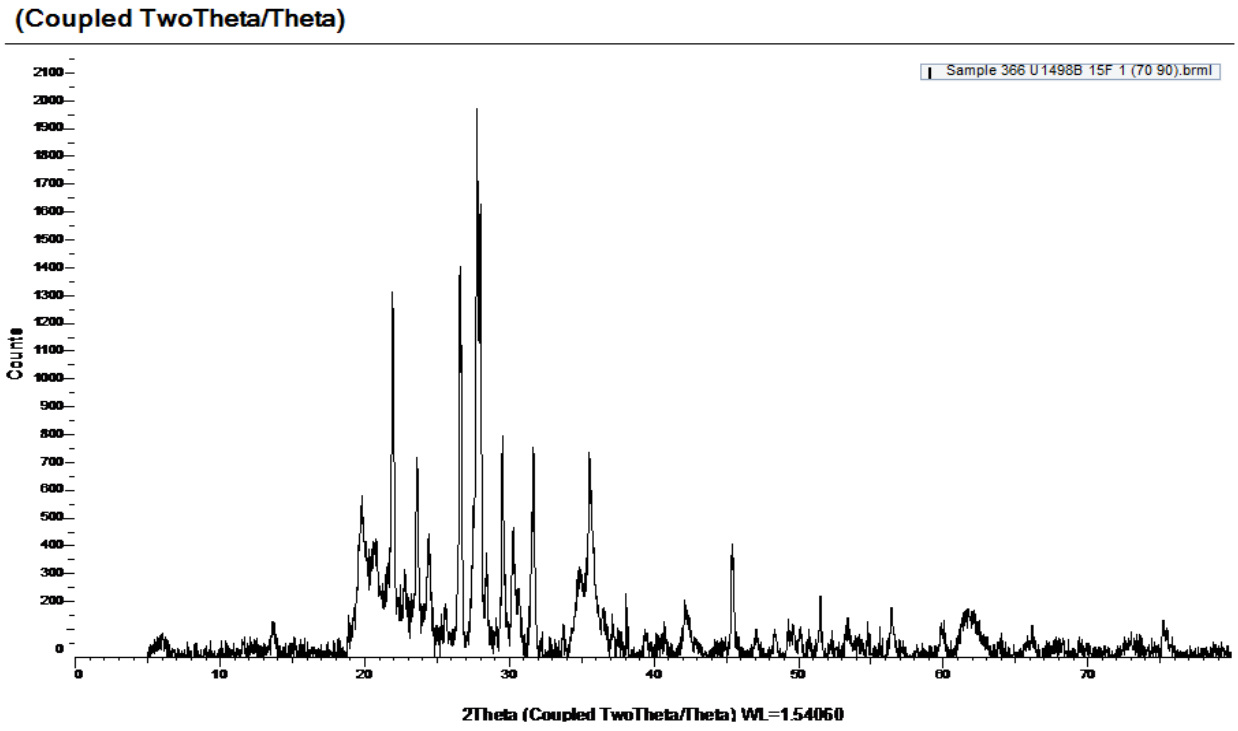

Fig. 9. Group D consists of U1498A-15R-01 (70 – 90 cm) to show the difference between this scan and the previous groups; A, B and C.

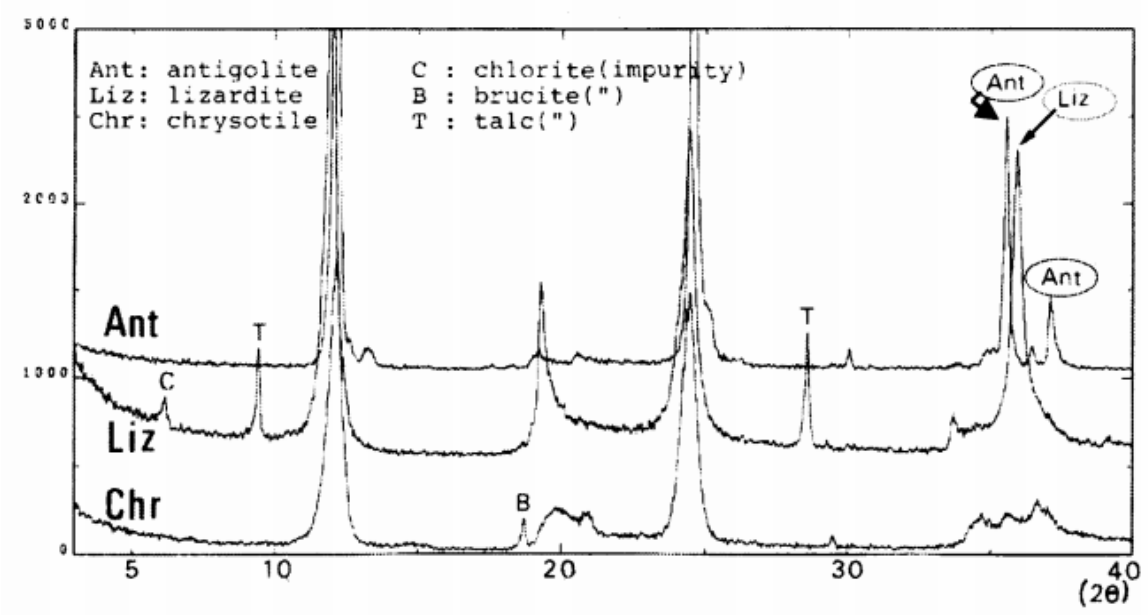

Fig. 10. Kohyama (2007) used these superimposed spectra of the three major serpentine minerals to differentiate between lizardite, antigorite, and chrysotile in powder XRD. "X-ray diffraction patterns of three polytypes of serpentine minerals. Circles indicate diffraction peaks effective for discrimination of each mineral." (Kohyama 2007).

2.3.3 Raman Analysis

The same crushed samples that were processed for XRD analysis were also analyzed using the Kaiser 785 nm micro-Raman spectrometry system. Samples were pressed between two glass slides, flattened, and then placed into the sample holder of the Raman system. After the sample was loaded, the 50x objective lens on the microscope was used to bring the sample into focus. A random spot was then picked for 5 separate 20-point count scans. We used a motorized sample stage with a joystick controller to maneuver the sample stage around. A photo of the area chosen for analysis was taken and the Raman system was set to acquire 100 scans per area. A point-count method was applied to the sample, which allows for a Raman spectrum to be obtained for each point during a scan. This produces a mineral map of the area analyzed. This method is applied if there is material on top of other material, so penetration depth can be

controlled, or if one is trying to gather a quantitative amount. Unfortunately, scans were unsuitable for mineral identification owing to strong fluorescence. This could have been due to organic matter, which resulted in too large a background to see an identifiable spectrum.

Data was processed in “HoloGRAMS 785nm” and converted into a spectrum for comparison to the Raman Spectrum database (*RRUFF*) and matched measured peak positions and widths to plausible mineralogy as compared with the XRD scans. The program HoloGRAMS 785nm also allowed for point count (an image is taken and overlaid with a grid of points then the object at each point is identified) measurements and photos of the sample selection to take place.

2.4 Methods, Analytical Techniques, and Comparisons

2.4.1 XRD Analytical Technique & Effectiveness

The puck containing the sample was placed in the XRD diffractometer where x-rays collide with the sample, while the sample is spinning, so that the x-rays hit the sample at every angle to produce an XRD pattern or a scan. The scan shows a series of peaks that correlate mathematically with spacings between planes of atoms in the mineral crystal (*Attard's Minerals, 2020*). These can be used to identify the mineral. XRD and Raman techniques both have the same function; to identify the mineral composition of the samples. The difference between the two methods is that XRD uses molecular structural differences to identify the minerals, and Raman spectrometry detects the vibrational energy of Raman scattering in each mineral. Because of the capabilities of the two methods, the methods were to be used to complement each other and to point out key mineralogy differences if any were present. However, the Raman data was not useful due to the high fluorescence of the samples tested (Fig. 19).

2.4.2 Errors, Bias, and Improvements

Shifts in peaks in XRD spectra from standards in the databases used for mineral identification in the XRD computer programs (Diffrac.eva & Topas) made identification of some accessory minerals difficult. The mineral phases that were being identified do contain a range of compositions, so minor shifts in degrees 2θ were expected (Lavina et al. 2014). The problem during Raman measurements was that possible presence of biological material resulted in too much fluorescence to permit identification of discrete minerals.

2.4.3. Research Limitations

Limitations regarding the XRD method were a consequence of mineralogical complexity of the samples and chemical variability of the minerals present.

Limitations regarding the Raman method were based on the samples' being heterogeneous, which caused a large sum of scans to possess a large hump in the spectrogram (Fig. 18), this was caused by fluorescence. Also, certain mineral phases can possess a greater Raman cross-section while other mineral phases can be overshadowed by an overwhelming spectra signal.

2.4.2 Raman Analytical Technique & Effectiveness

Radiation interacts with a mineral's atoms in two ways, by transmitting through the mineral or by reflecting (scattering) off the mineral either elastically (Rayleigh scattering) or inelastically (Raman scattering). When a laser or monochromatic radiation illuminates the mineral, the atoms begin to vibrate and heat up, causing them to absorb and then scatter off photons of specific wavelengths, related to the energy of vibration being excited. The scattered light is reflected by certain planes causing radiation to bounce off those planes that have been

created within the molecular structure of a mineral, radiation is polarized within the structure of the mineral. The spectrograph produced by the resulting change in energy created is a measure of the frequency of the vibration of a molecule. If the molecule moves at a high frequency, its atoms are strongly held together, and it produces a significant change in energy. If the molecule moves at a low frequency its atoms are loosely held together, producing a small change in energy. This type of analysis was ineffective for our samples due to high fluorescence likely caused by organic material in the sample that masked the wavelength shifts of minerals.

3.0 RESULTS

3.1 Reasoning for Comparisons Between XRD & Raman

3.1.1 XRD Results

The diffractograms revealed lizardite as the dominant mineral in three of four sample groups that were scanned with XRD. The fourth group (D) was dominated by feldspar minerals and pyroxene (Table 1). Reference table 1 for the complete list of minerals identified during this study.

The following figures show angles 2-theta increasing to the right on the x axes, and X-Ray counts increasing upward on the y-axis for each group along with the minerals matched per sample scan (Figs. 11-21):

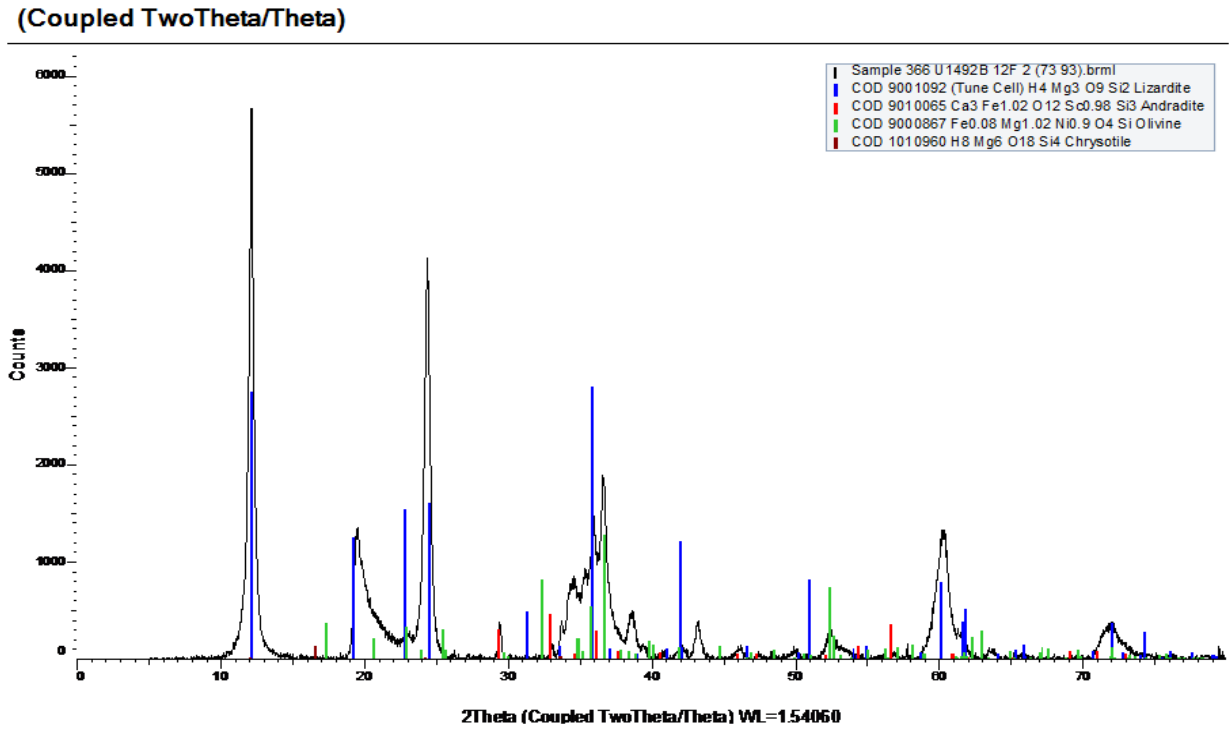

Fig. 11. Group A, U1492B-12F-2 (73-93 cm); consists of lizardite, andradite, olivine, and chrysotile.

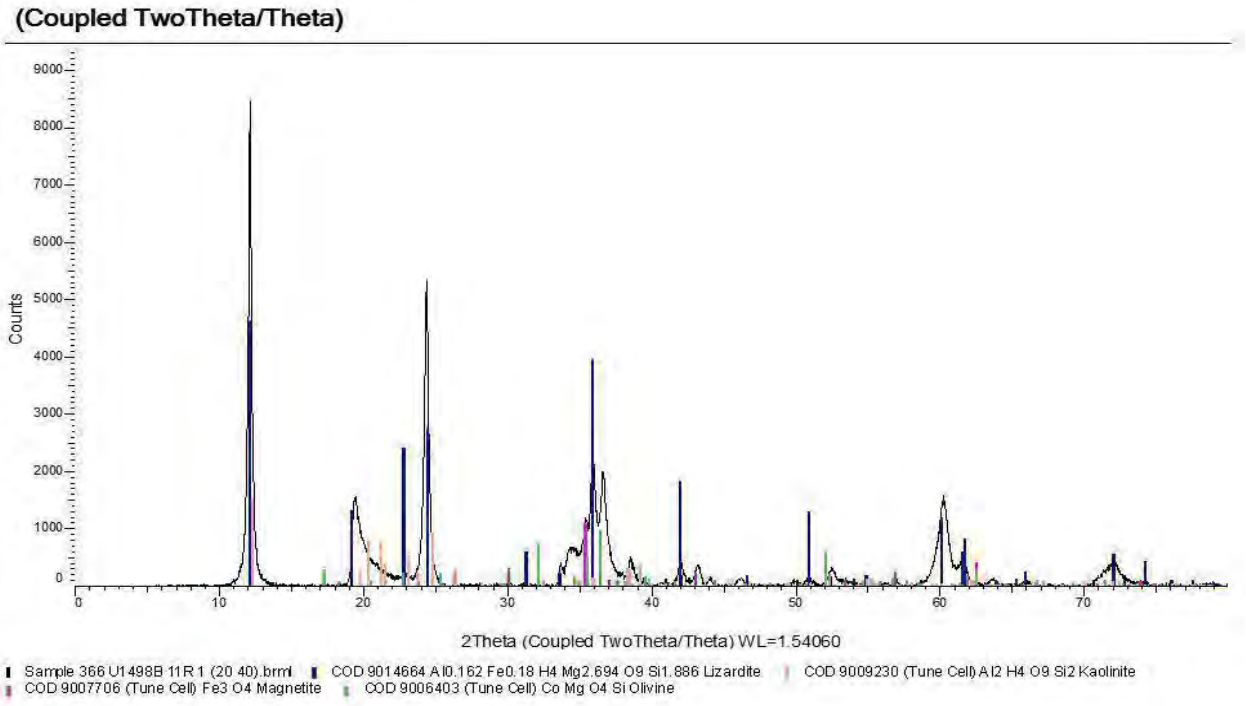

Fig. 12. Group A, U1498B-11R-4 (20-40 cm) consists of lizardite, olivine, calcite, garnet, and halite.

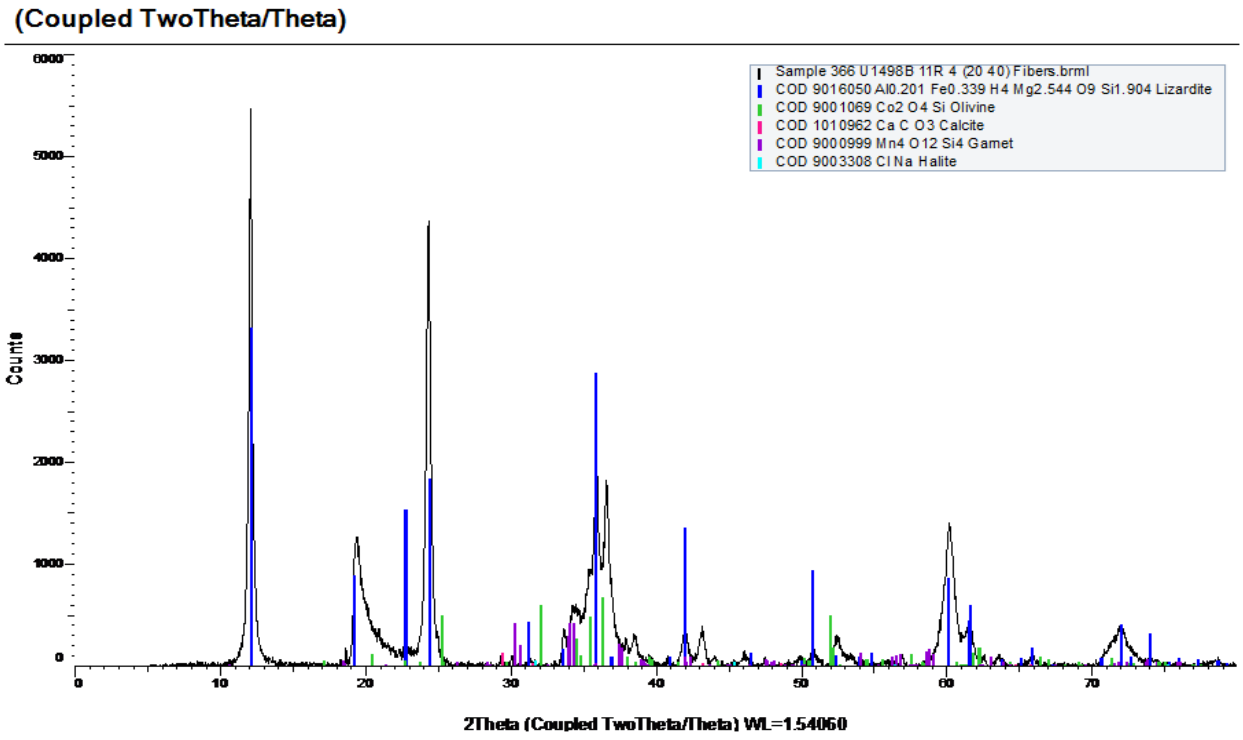

Fig. 13. Group A, U1498B-11R-4 (20-40 cm) Fibers consists of lizardite, kaolinite, magnetite, and olivine.

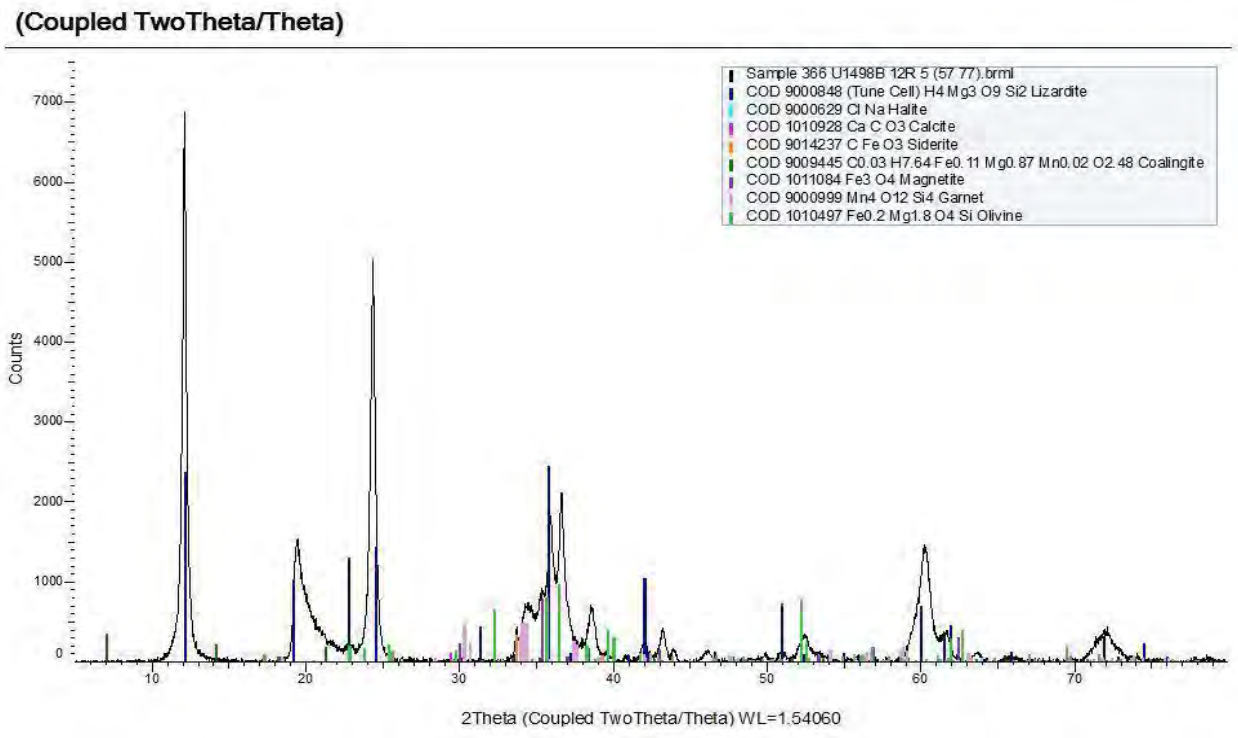

Fig. 14. Group A, U1498B 12 R 5 (57 77) consists of lizardite, halite, calcite, siderite, coalingite, magnetite, garnet, and olivine.

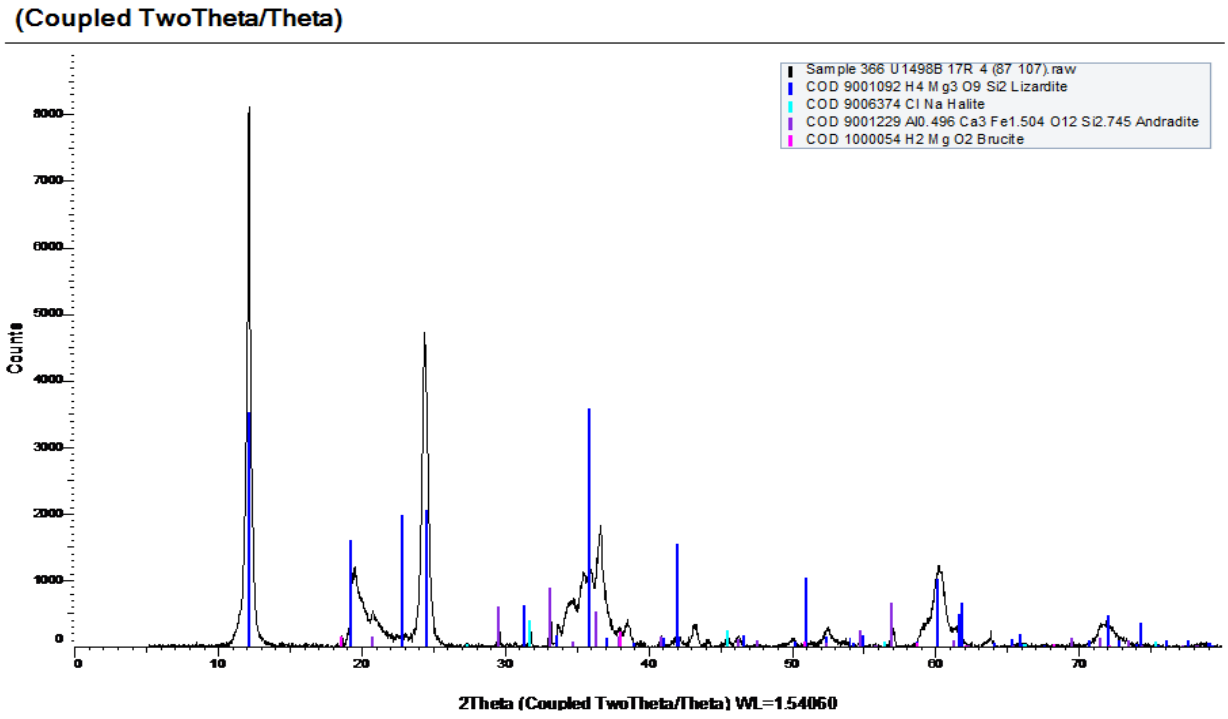

Fig. 15. Group A, U1498B-17R-4 (87-107 cm) consists of lizardite, halite, andradite, and brucite.

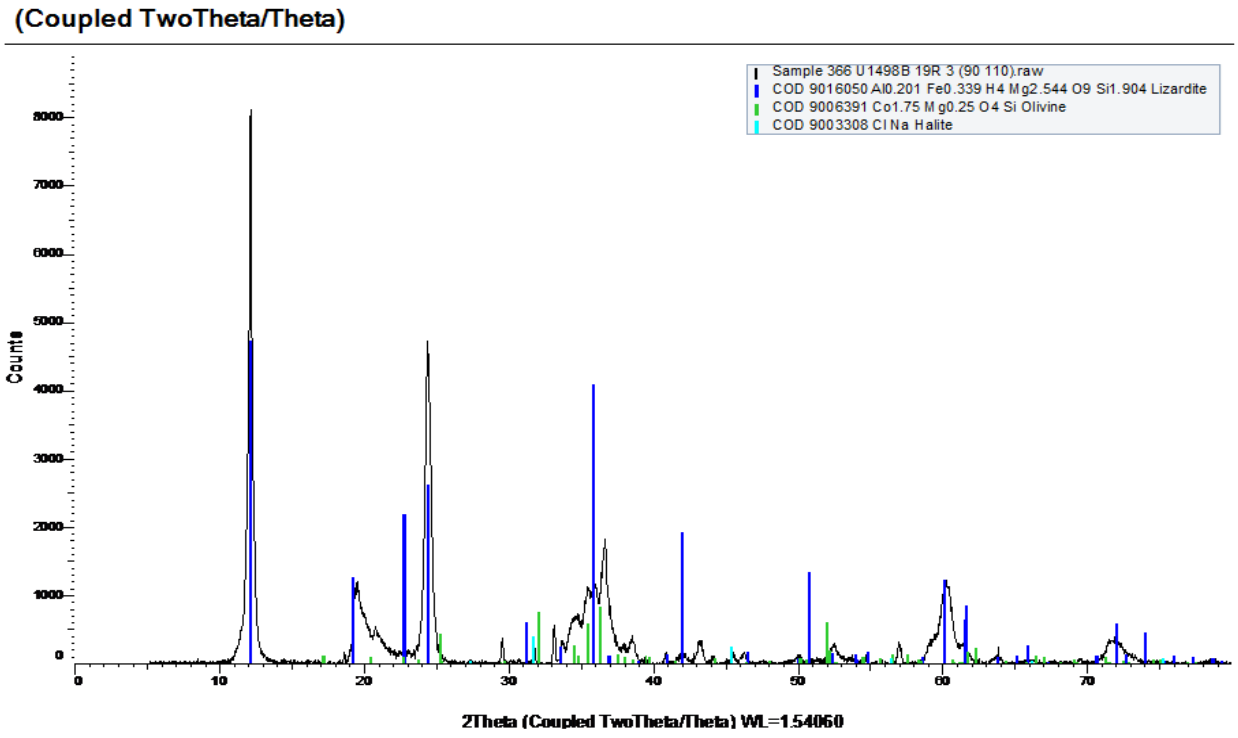

Fig. 16. Group B, U1498B 19R 3 (90 110) consists of lizardite, olivine, and halite.

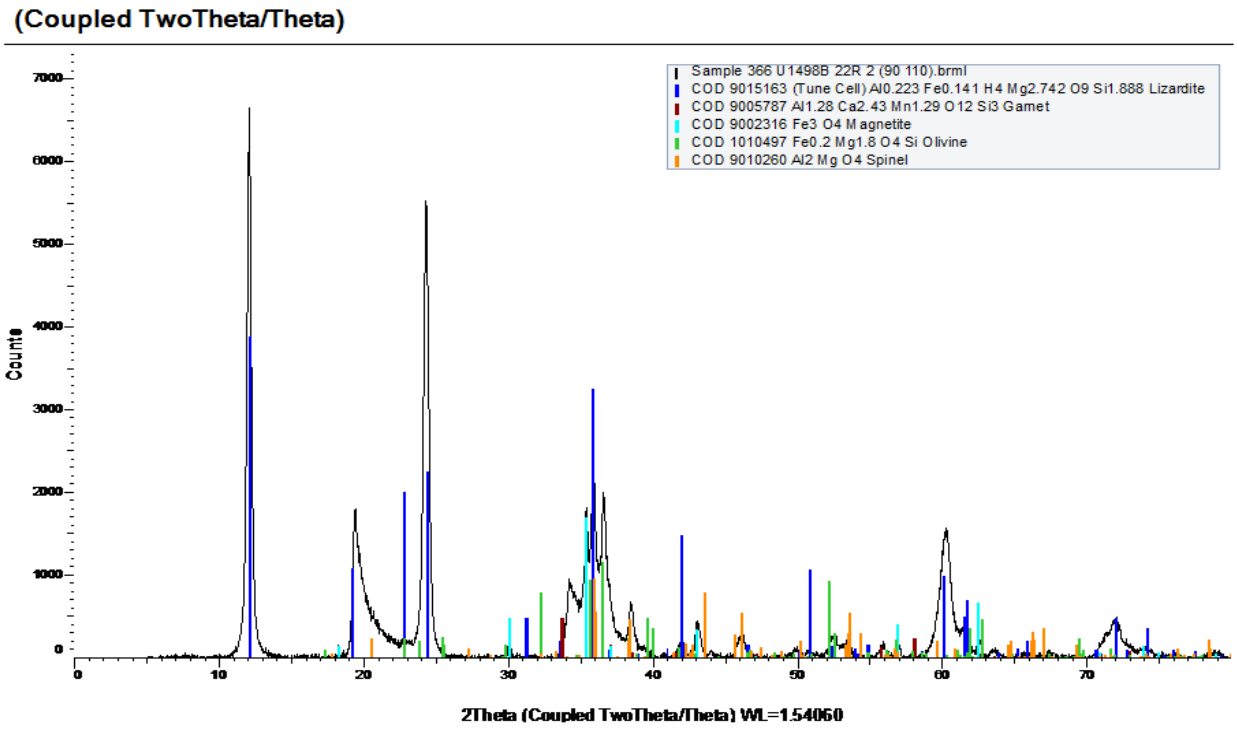

Fig. 17. Group B, U1498B-22R-2 (90-110 cm) consists of lizardite, garnet, magnetite, olivine, and spinel.

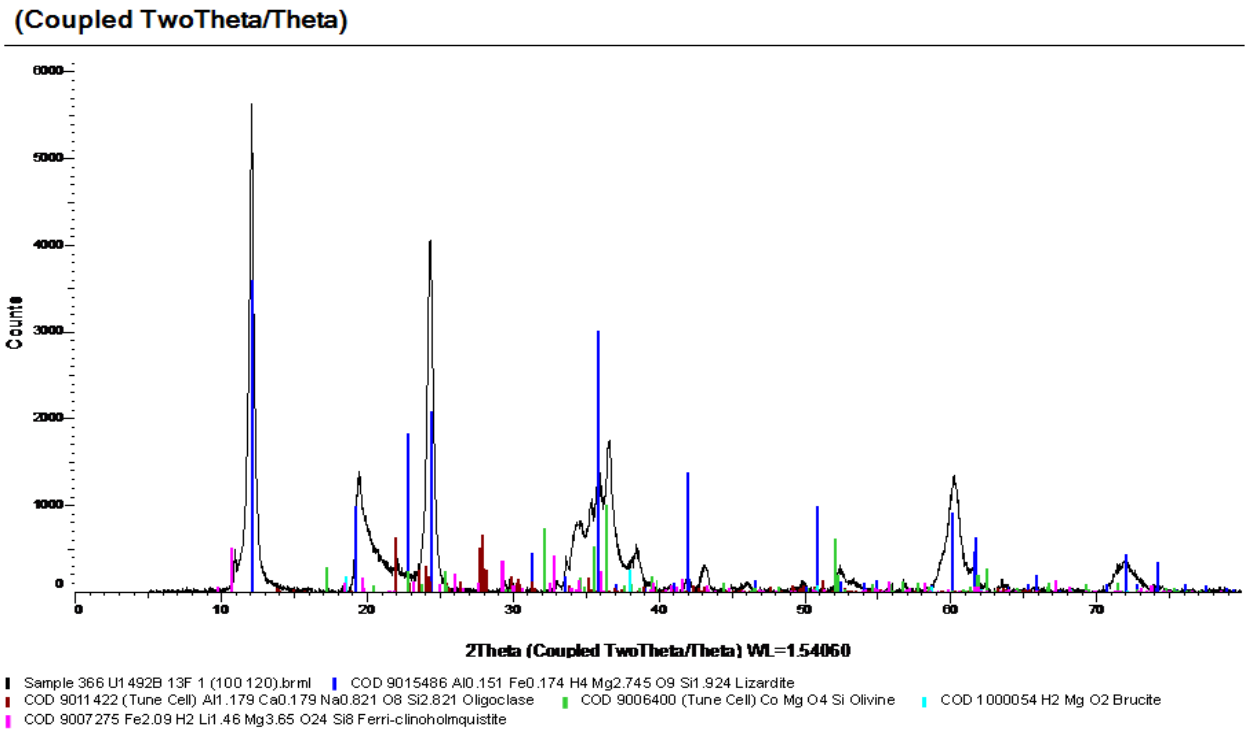

Fig. 18. Group C, U1492B 13F 1 (100,120) initially presented an unidentifiable peak in the scan that was later identified to be ferri-clinoholmquistite, the sample also consists of lizardite, oligoclase, olivine, and brucite.

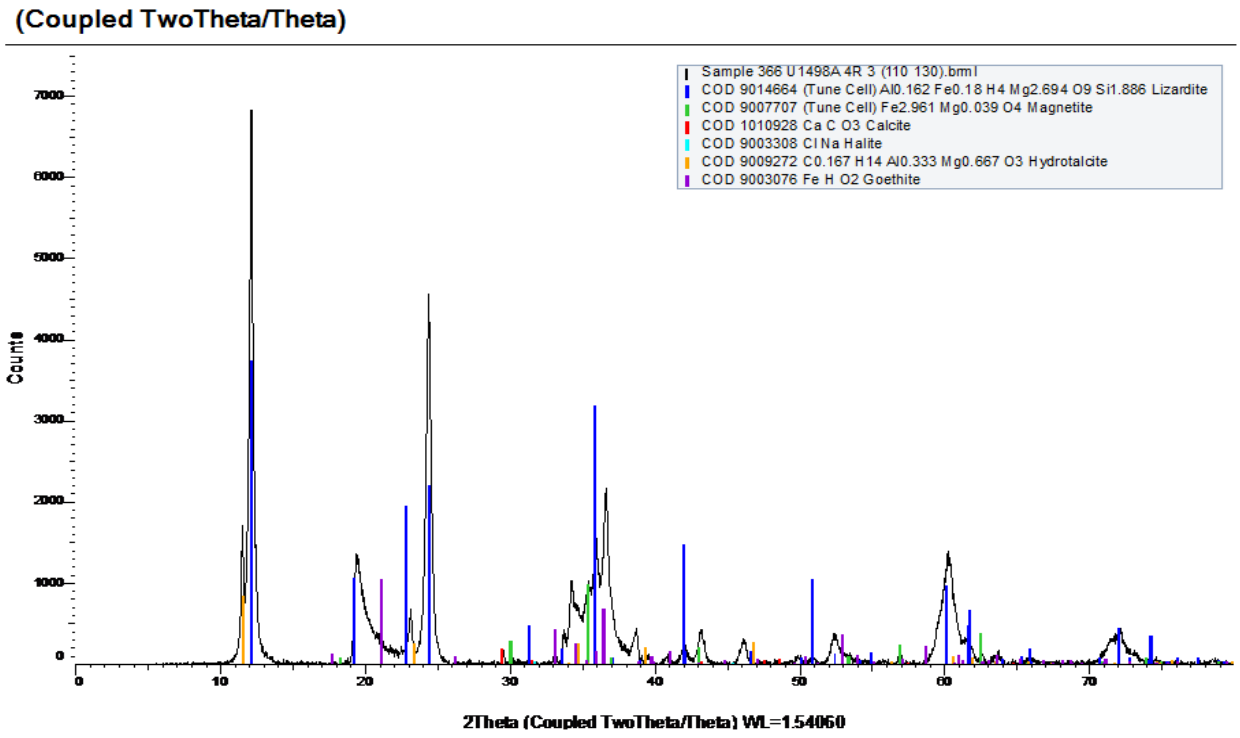

Fig. 19. Group C, U1498A 4R 3 (110, 130) the sample also consists of lizardite magnetite, calcite, halite, goethite, and hydrotalcite.

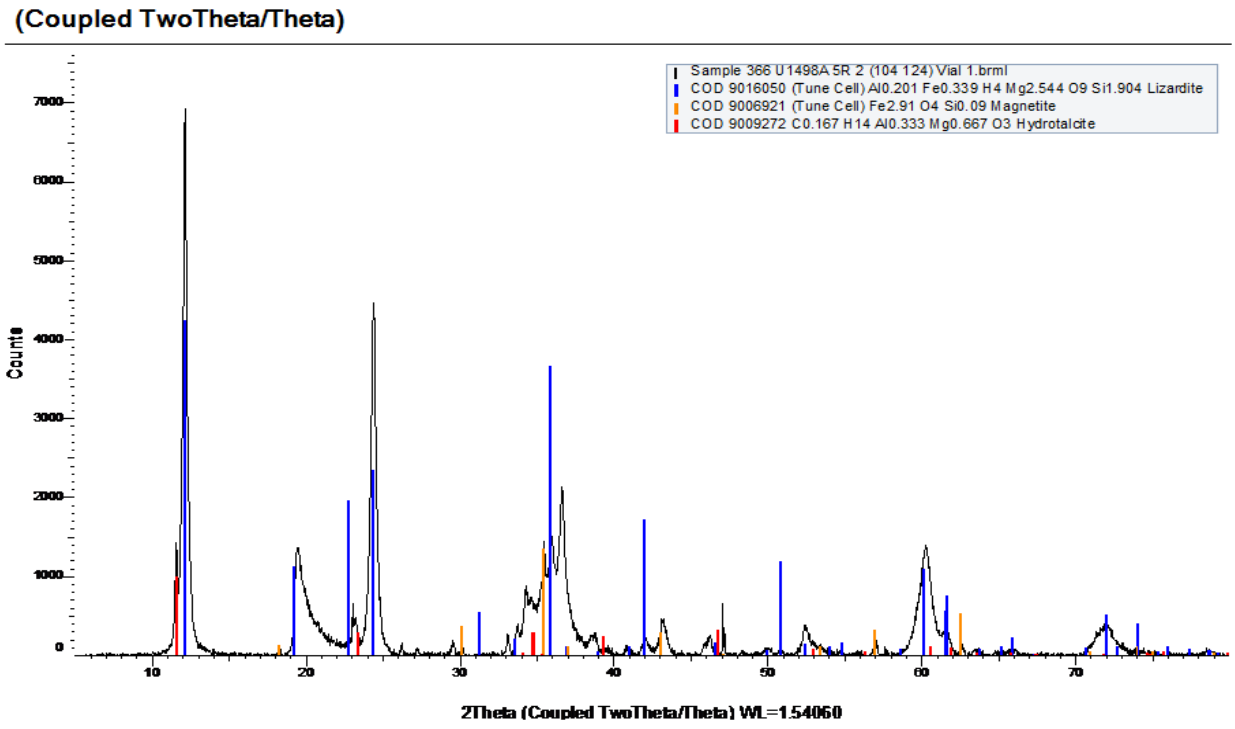

Fig. 20. Group C, U1498A-5R-2 (104-124cm) vial 1 initially presented an unidentifiable peak in the scan that was later identified to be hydrotalcite, the sample also consists of lizardite and magnetite.

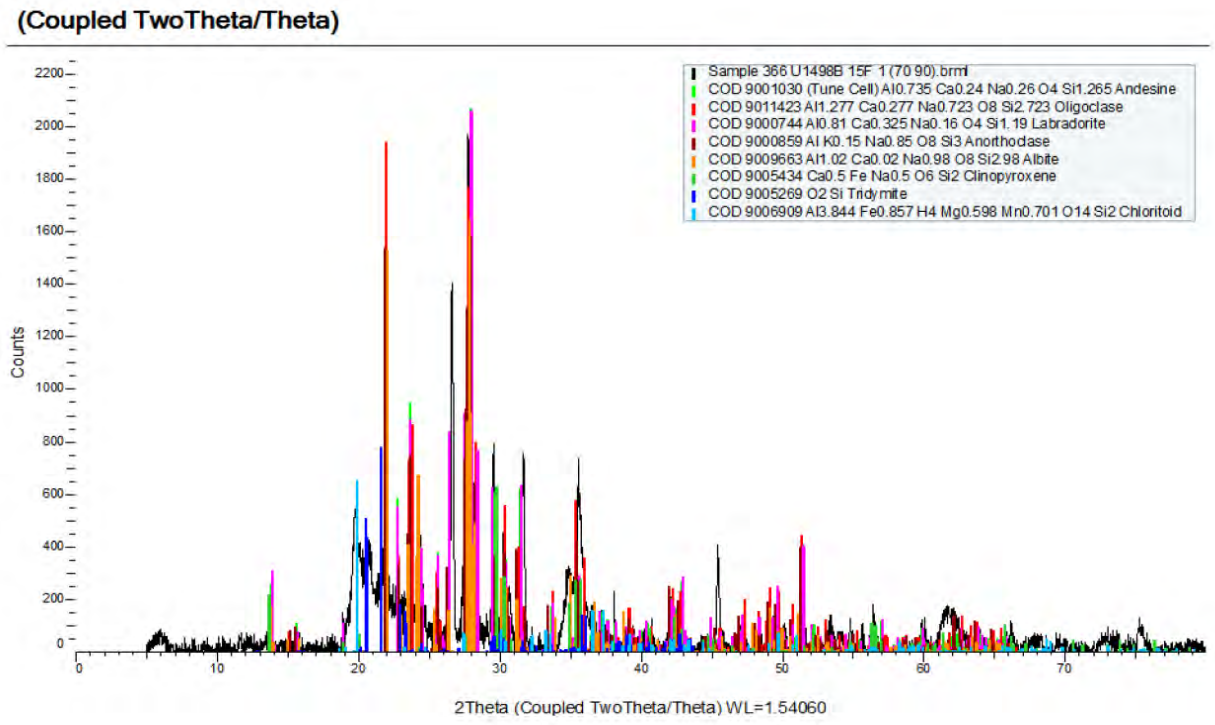

Fig. 21. Group D, U1498A 15 R 1 (70 90), this scan was distinct from the rest as it showed a dominant amount of feldspars; andesine, oligoclase, labradorite, and albite. The sample is also dominant in clinopyroxene with accessory minerals; tridymite and chloritoid.

3.1.2 Raman Results

Scans given through the use of the program HoloGRAMS 785nm and the Raman Spectrometer were indecipherable. This is due to the samples' being heterogeneous, containing different amounts of different minerals and different clast sizes and fluorescing likely because of the presence of organic material. The heterogeneity of the samples produced a large sum of scans creating a large hump in the spectrogram (Fig. 22), which was caused by fluorescence possibly related to organic material in the samples, certain mineral phases possess greater Raman cross-sections and other mineral phases are overshadowed by the overwhelming spectra signal. The point-count method did not work because: a) some mineral phases have greater Raman cross-sections that others and their signal overwhelms the spectra; and b) some mineral phases are a lot

more abundant than others, at times several orders of magnitude, which would require using high magnification and a small step size leading to an unreasonably long amount of measurement time.

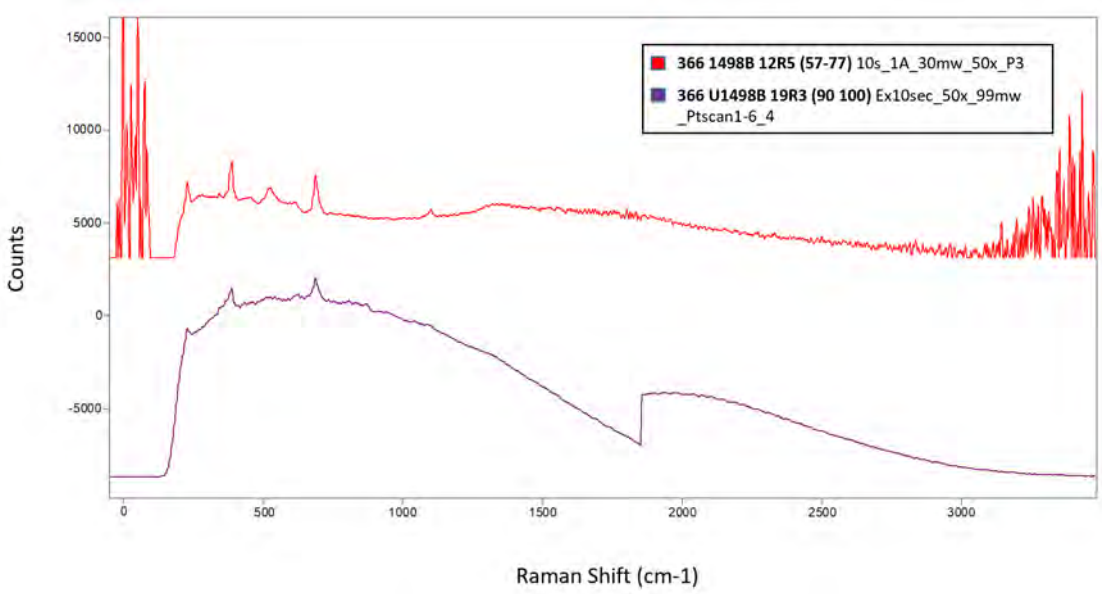

Fig 22. Two results from two samples measured at 10 seconds each and 50x. 366 U1498B (57 77) presented low fluorescence and 366 U1498B-19R-03 (90 – 100 cm) presented high fluorescence.

3.2 Analytical Results

XRD produced ten scans indicating a high abundance of lizardite throughout all scans and one sample, 366 U1498A-15F-01 (70 – 90 cm), indicating antigorite and andesine. The table below presents the mineral composition of the 11 samples presented during this study. The Raman analysis produced a multitude of scans containing a high abundance of fluorescence that made many scans hard to decipher. Therefore, XRD scans were used exclusively to identify the mineralogy of the samples.

Table 1. Compilation of all samples and what is dominant (D) present (P) and possibly present (PP) in the samples.

Samples	Minerals->	Lizardite	Chrysotile	Olivine	Spinel	Magnetite	Brucite	Andradite	Garnet	Ferri-clinoholuusite	Calcite	Coalingite	Sjoerite	Kaolinite	Hydrotalcite	Geothite	Oligoclase	Andesine	Labradorite	Anorthoclase	Albite	Clinopyroxene	Tridymite	Chlorritoid	Halite
Group A																									
366 U1492B 12F 2 (73 93)		D	P	P		PP		P																	PP
366 U1498B 11R 4 (20 40)		D	P	P		P								P											PP
366 U1498B 11R 4 (20 40) Fibers		D	P	P		PP			P		P														P
366 U1498B 12R 5 (57 77)		D		P		P			P		P		P												P
366 U1498B 17R 4 (87 107)		D		PP		PP	P	P																	P
Group B																									
366 U1492B 13F 1 (100 120)		D		P		PP	P			P							P								PP
366 U1498A 4R 3 (110 130)		D		PP		P					P				P	P									P
366 U1498A 5R 2 (104 124) Vial 1		D		PP		P									P										PP
Group C																									
366 U1498B 19R 3 (90 100)		D		P		PP																			P
366 U1498B 22R 2 (90 110)		D		P	P	P			P																PP
Group D																									
366 U1498A 15F 1 (70 90)																	P	P	P	P	P	P	P	P	

4.0 DISCUSSION

The primary findings of 11 drill cores samples recovered during IODP Expedition 366 from two active serpentinite mud volcanoes; Yinazao and Fantangisña Seamounts indicate that there is little difference in the mineralogic composition of the samples from this study. Table 1 shows the dominant, present, and possibly present minerals within the 4 groups sampled from the Mariana forearc. Across 11 samples, mantle minerals, secondary alterations of mantle minerals, volcanic ash, and halite from dehydration of seawater were present. Lizardite was found in 10 of the 11 samples. These minerals show that Group D consists of different materials from Groups A, B, and C and are consistent with pelagic sediments found on the Mariana forearc which likely represent volcanic ashfall, submarine landslides, possibly dust from Asia, and microorganism remains.

4.1 Mineral Comparison to Smear Slides for U1498B

Figure F10. Downhole changes in mud composition, Hole U1498B. D = dominant (>50%), A = abundant (20%–50%), C = common (10%–20%), R = rare (1%–10%), Tr = trace (<1%). The sample at 200.21 mbsf is scratched from a green metabasite.

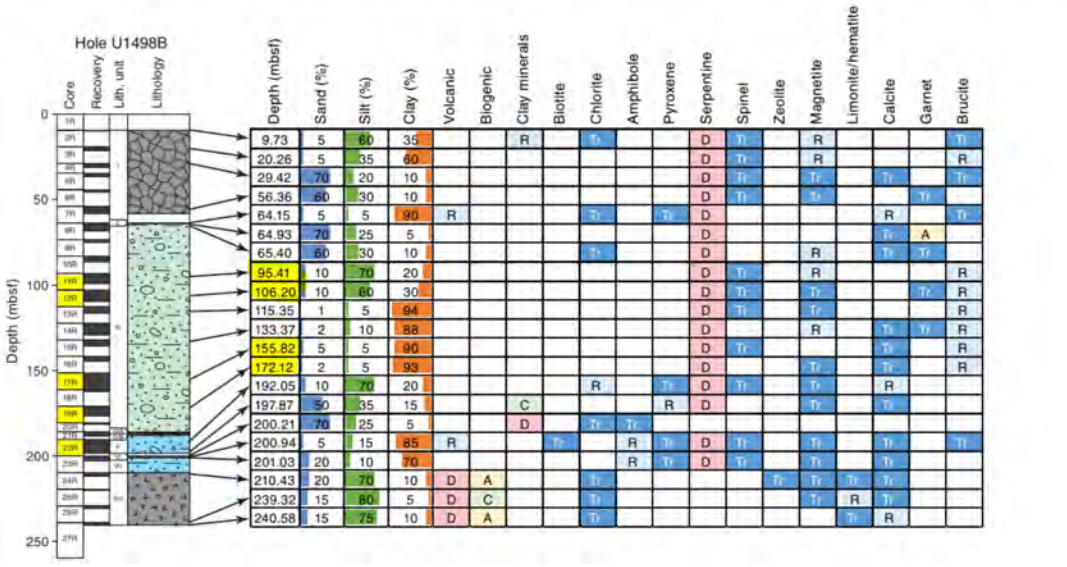

Fig. 23. Smear slide data for U1498B (Fryer et. al 2016), highlighted depths are samples presented during this study to use as a comparison against gathered mineralogy composition.

Aboard IODP Expedition 366 smear slide analysis was conducted to identify minerals present for U1498B (Fig. 20). This data was compared against XRD findings from this study (Figs. 11-21). Key mineralogical differences to be noted are that spinel, garnet, and brucite were deemed minor phases present in the smear slide testing in the five samples that were tested in both smear slide testing and XRD testing. There was also biogenic material, possibly a silicate; siliceous micro fauna compositional variability was found during the smear slide examinations. Spinel was found to be present in 366 U1498B-22R-02 (90 – 110 cm), this could be due to the much smaller sample size taken for the smear slides versus the amount taken for XRD analysis for this study. The difference in techniques showed that although the smear slide observation was able to gather data from material in which the ship-board scientists had a particular interest, the XRD data was able to confirm bulk mineralogy of the samples whilst also identifying minerals present in smaller amounts as well as permitting differentiation between specific serpentinite minerals. For instance, it was not possible to distinguish between lizardite and antigorite in the smear slides.

4.2 This Study Vs. Shipboard XRD Analysis

Due to the lack of a functioning XRD aboard IODP Expedition 366 during the expedition, the land based XRD for this study was used to determine the mineralogy of the samples. However, an earlier IODP Expedition (#362) had a functioning XRD on board. To compare our XRD approach with the IODP shipboard one, we looked at their protocol (McNeill et al., 2017). On IODP Expedition 362 they crushed their samples for 3 minutes with a ball mill after vacuum drying the samples and used the Bruker D4 Endeavor diffractometer, which is very similar to the Bruker D8 Advanced XRD housed in the University of Manoa campus. The data

collection settings aboard Expedition 362 were Voltage = 40 kV., Current = 40 mA., Tube anode = Cu., Wavelength = 1.54060 Å (Kα1) and 1.54443 Å (Kα2).,Step spacing = 0.008°2θ., Scan step time = 0.648 s, Divergent slit = automatic., Irradiated length = 10 mm , Scanning range = 2°–40°2θ, Spinning = yes. (McNeill et al., 2017) vs. our stage of spinner phi with air scatter and scanned at coupled 2θ/θ, 5-80°/sec/0.02°, each scan lasting 1 hour. Both methods used the (Bruker software package) DIFFRAC.EVA to determine quantitative and qualitative data regarding mineralogy of the samples, respectively (McNeill et al., 2017). There is no real way of knowing if the settings chosen during IODP Expedition 362 were superior to our settings for mineral identification as the primary function for both parties was to identify mineralogy of samples which they and we achieved. However, using XRD is superior to smear slide testing. During smear slide testing the sample size is exceedingly small and limited because a toothpick is used to gather the sample. Also, the identification of minerals is limited by the knowledge of the analyst. During XRD a larger sample size is taken and ground up. With a larger sample size, a more accurate representation of the bulk samples is gathered.

4.3 Future Testing Recommendations

Recommendations for future testing of materials used in this study would be to isolate single crystals of different minerals and do single crystal diffraction to help define the specific composition of the minerals. This would allow us to explain with ease why peaks may be shifted based on slight compositional differences. Another recommendation would be to conduct Raman scans for organic material since there was a significant amount of fluorescence observed during the Raman trials. Lastly, by isolating individual grains to get the elemental composition by using a high-resolution scanning electron microscope to gain an analysis of areas as small as ~15

microns and get a spectral analysis of elements present, this could aid in the verification of mineralogy and gather quantitative results.

4.4 Mineral Processes & Their Meanings

In many cases knowing how a mineral was created allows for a greater understanding of the physiological and chemical processes of the area in the study. In this study knowing these processes (Table 2) will aid us further in understanding the geological processes taking place within and around Yinazao and Fantangisña Seamounts.

Table 2. Description of minerals present in the samples of this study and likelihood of occurrence in Mariana forearc serpentinite mudflows.

Lizardite	Hydration product of peridotite, a low-med-temperature serpentine (Evans et al., 2012), and would be derived from the forearc mantle rocks.
Antigorite	Hydration product of peridotite, a higher-temperature serpentine mineral (Evans et al., 2012), and would be derived from the forearc mantle rocks.
Chrysotile	Hydration product of peridotite, a low-temperature serpentine, (Evans et al., 2012), and would be derived from the forearc mantle rocks.
Andesine	Plagioclase feldspar with 30 to 50% Ca. Typical of andesitic lavas that erupt in the Mariana Island Arc (e.g., Natland and Tarney, 1981, Reagan et al, 2003), and could be carried in ash to the forearc via local winds or come from comminution of lavas from the forearc crust.
Olivine	Dominant upper mantle mafic silicate mineral in the Mariana forearc (Saboda et al., 1992), and is present in partially serpentinized forearc mantle rock clasts in serpentine mudflows (Saboda et al., 1992, Fryer et al., 1999).
Andradite	A garnet mineral with cations of Ca and Fe, green color, and generally hydrated and is present in partially serpentinized forearc mantle rock clasts in serpentine mudflows (Fryer and Mottl, 1992).
Kaolinite	Clay mineral, a common alteration product of serpentine (e.g., Nozaka et al., 2008).
Magnetite	An iron oxide commonly formed during serpentinization (Beard et al., 2009), is present in serpentinized forearc mantle rock clasts in serpentine mudflows (Fryer et al., 2018).

Garnet	Garnets are typical of minor mineral phases in the mantle; it has been observed that most garnets found in the serpentine mudflow material are hydrated; this means that they also have interacted with fluids likely from the subducted plate (Fryer and Mottl, 1992).
Halite	Also known as rock salt, it forms via simple evaporation of saltwater (e.g., King, 2020), and forms in the serpentinite mudflows as the drill cores dry.
Calcite	Calcium carbonate is commonly formed in association with serpentinite muds and as chimney structures at springs on the summits of serpentinite mud volcanoes of the Mariana forearc by interaction of pore fluids with seawater (Fryer et al., 1999).
Brucite	A magnesium hydrate mineral that forms during the first stage of hydration of peridotites (Beard et al., 2009) and can also form chimney structures at springs on serpentinite mud volcanoes close to the Mariana trench by interaction of pore fluids with seawater (Fryer et al., 1999).
Oligoclase	Plagioclase feldspar with 10-30% Ca. Typical of andesitic lavas that erupt in the more silicic of the Mariana Island Arc eruptions (e.g., Natland and Tarnery, 1981, Reagan et al., 2003) and could be carried in ash to the forearc via local winds or come from comminution of lavas from the forearc crust.
Coalingite	A Mg, Fe hydrated, hydroxy, carbonate, a common alteration product of serpentine and is found in serpentinite mudflows (e.g., Fryer and Mottl, 1992).
Siderite	An Fe-carbonate mineral, common in reducing environments and is favored as a precipitate as dissolved inorganic carbon in pore fluids increase (e.g., Koo and Kim, 2020), such as in serpentinite mudflows (e.g., Mottl, 1992).
Spinel	A common accessory mineral in peridotite, would be present in partially serpentinized forearc mantle rock clasts in serpentine mudflows (e.g., Saboda et al., 1992, Fryer et al., 2018).
Ferri-clinoholmquistite	A Li-bearing, Fe amphibole (Caballero et al., 1998), unusual in this locality, but possibly associated with alteration of mantle peridotic rocks (e.g., Arai, 1986), or altered forearc crustal rocks because the Li content suggests derivation from the subducted-slab-derived fluids (e.g., Benton et al., 2004)

Hydrotalcite	An Mg, Al hydrated, hydroxy, carbonate found in Mariana serpentinite mudflows as a common alteration product of serpentine (e.g., Fryer and Mottl, 1992).
Goethite	A Fe hydroxide mineral caused by alteration of iron-bearing minerals that are most common in mafic rocks, so could form from altered Pacific Plate basalts or gabbros (e.g., Meijer et al., 198) from the subduction channel, from altered forearc mafic rocks entrained in the serpentinite mudflows or from alteration of serpentine itself, within the mudflows (Fryer and Mottl, 1992).
Andesine	Plagioclase feldspar with 30-50% Ca. Typical of andesitic lavas such as eruptions in the Mariana Island Arc (e.g., Wood et al., 1981, Reagan et al, 2003) and can be carried in ash to the forearc via local winds, or come from comminution of lavas from the forearc crust.
Labradorite	Plagioclase feldspar with 50% Ca. Typical of andesitic lavas that erupt in the more silicic of the Mariana Island Arc eruptions (e.g., Wood et al., 1981, Reagan et al, 2003) and can be carried in ash to the forearc via local winds, or come from comminution of lavas from the forearc crust.
Anorthoclase	Alkali feldspar (with Na, K cations). Typical of the more silicic lavas of the Mariana Island Arc eruptions (e.g., Wood et al., 1981, Reagan et al, 2003) and can be carried in ash to the forearc via local winds, or come from comminution of lavas from the forearc crust.
Albite	Plagioclase feldspar with 0-10% Ca. Typical of the more silicic lavas of the Mariana Island Arc eruptions (e.g., Wood et al., 1981, Reagan et al., 2003), and can be carried in ash to the forearc via local winds, or come from comminution of lavas from the forearc crust.
Clinopyroxene	General term for pyroxene that is monoclinic in crystal system and generally has a mixture of Ca, Mg, and Fe cations and is common in Mariana basaltic lavas (e.g., Meijer et al., 1981, Reagan et al., 2003), thus could be carried in ash to the forearc via local winds, or come from comminution of lavas from the forearc crust.
Tridymite	A form of SiO_2 stable between 870°C 1470 °C occurs in lavas such as those of the Mariana Island Arc (e.g., Reagan et al., 2003), thus could be carried in ash to the forearc via local winds.
Chloritoid	Fe, Mg, Mn, and Al silicate hydroxide. Can form in altered pillow lavas or hydrothermal systems, but more common in metamorphic rocks, thus it could have come from Pacific Plate seamount fragments from the subduction channel, or come from altered comminuted lavas from the forearc crust (Fryer et al., 2020).

4.5 Relevance of Serpentinite Mud Volcanism

The Mariana forearc serpentinite mud volcanoes have been active for an unknown amount of time, however, it is speculated that they have been active since the Philippine Sea Plate (overriding plate) began overriding the Pacific Plate (subducting plate) about 50 million years ago (Fryer, 2012) . Serpentinization is attracting attention in the microbiology community because it has been suggested that serpentinization environments may be where life originated (Fryer, 2012; Fryer et al., 2020). The serpentinization process creates an extreme reducing environment with high pH, and provides nutrients needed for microorganisms to survive and thrive. The conditions under which serpentinization takes place allows peridotite to produce hydrogen-rich fluids that are able to react with dissolved carbon dioxide to create methane, the hydrogen and methane created are a source of energy for chemoautotrophic organisms; meanwhile, anaerobic oxidation of methane generates hydrogen sulfide used by sulfide oxidizing bacteria that are symbiotic with chemosynthetic organisms (Ohara et al., 2011). Although the Mariana forearc is the only location where such processes are currently active on Earth, there are similar deposits world-wide and in deposits of materials as old as 3.8 billion years ago (Fryer, 2012; Fryer et al., 2020).

5.0 CONCLUSIONS

These data are consistent with the overall findings from onboard studies of cores from Mariana forearc serpentinite mud volcanoes of IODP Expedition 366. Because no XRD analytical capability was available on board the ship during the expedition, these data will provide a basis for future studies by expedition scientists, as they are the first XRD data obtained for IODP Expedition 366 samples. Lizardite was dominant in groups A, B, and C. Olivine, halite and calcite were prominent minerals in groups A, B and C.

Groups A, and B were identical despite their being composed of samples from two different seamounts but did not signify any large changes between the samples, which suggests that geological processes were similar at both seamounts. The mineralogy of the mudflows has not changed greatly over time and the one outlier sample; group D's diversity was different because it clearly represents sediments underlying the flank of Fantangisña Seamount. Some of this sediment was introduced as a result of contribution of ash from explosive volcanic events from the nearby Mariana Island Arc volcanoes because feldspar and pyroxene were dominant in the sample. These two minerals are the dominant components of Mariana Arc lavas. This is important because if researchers are interested in dating the sequence of mudflows in that area they could resample the core and date the ash radiometrically or by microfossil age ranges, but the fact that the deep sites on Fantangisña Seamount are covered in thick sediment (Fryer et al., 2018) indicates its older age. The similarity of the mineralogy between samples of serpentinite mud suggests the major underlying processes have not changed much over the life of the mud volcanoes so the extremophile Archaea found in the mudflows (Curtis et al., 2013) and the reducing and high-pH, extreme environment (Fryer et al., 1999) in these mud volcanoes probably existed throughout their lifetime.

During the identification process, there was one unidentified peak in group D, this is due to three possibilities; minerals could have been stacked on top of each other, the mineral could have been oriented a specific way, or due to feldspars having an exceptionally strong cleavage, the minerals could have been oriented the same way creating a larger peak. These minerals show that Group D consists of different materials from Groups A, B, and C and are consistent with pelagic sediments found on the Mariana forearc which likely represent volcanic ashfall, submarine landslides, possibly dust from Asia, and microorganism remains.

If the process by which the Mariana serpentinite mud volcanoes grew created an environment supportive of microbial life (Curtis et al., 2013), then the process by which similar deposits in similar geologic settings of the past (e.g., Lockwood 1971; 1972; Phipps, 1988; 2000; Pons et al. 2011) could also have supported microbial life. Since we know there are deposits throughout the world and throughout geological time that are similar to those of the Mariana forearc mud volcanoes, they too may have been conducive to microbial life. The next step in confirming or disproving whether microbial life began in serpentine environments would be to compare findings throughout the world and in ancient deposits. Then by deductive reasoning, we can say that serpentine mud volcanism at convergent margins in the early history of the Earth may have been one of the environments where life began on our planet. If the origin of life is related to serpentinization then we can expect that normal volcanic ash deposits on the surface of the earth might be a good environment for the origin of life and if eventually future expeditions are conducted, we can find evidence for a difference in microbial communities within the underlying ash.

LITERATURE CITED

"Search RRUFF Sample Data." *RRUFF*, rruff.info/.

"Identifying Minerals by X-Ray Diffraction." *Attard's Minerals*, https://attminerals.com/x-ray-diffraction-identifying-minerals.

Arai, S. (1986): K/Na variation in phlogopite and amphibole of upper mantle peridotites due to fractionation of the metasomatizing fluids. J. Geol., 96, 436-444.

Beard J. S., Frost, B. R., Fryer, P., McCaig, A., Searle, R., Ildefonse, B., Zinin, P., Sharma S. K., 2009, Onset and progression of serpentinization and magnetite formation in olivine-rich troctolite from IODP Hole U1309D. Journal of Petrology, 50(3):387-403.

Benton, L. D., Ryan, J. G., and Ivan P. Savov, 2004. Lithium abundance and isotope systematics of forearc serpentinites, Conical Seamount, Mariana forearc: Insights into the mechanics of slab-mantle exchange during subduction. Geochemistry, Geophysics, Geosystems, 5(8). https://doi.org/10.1029/2004GC000708

Boughton, P., 2015. "XRD for Analysing Powders." *XRD for Analysing Powders | Scientist Live*, 21 Dec. 2015, https://www.scientistlive.com/content/xrd-analysing-powders.

Caballero, J. M., Monge, A., L Iglesia, A., and TORNOS, F. 1998. Ferri-clinoholmquistite, Li2 (Fe2+, Mg)3 Fe23+ Si8O22 (OH)2, a new Li clinoamphibole from the Pedriza Massif, Sierra de Guadarrama, Spanish Central System. American Mineralogist, Volume 83, pages 167–171.

Evans, B. W., 2004. The serpentinite multisystem revisited: Chrysotile is metastable. Int. Geol. Rev. 46:479–506

Evans, B. W., Hattori, K. and Baronnet, A., 2012. Serpentinite: What, Why, Where? Elements, 9:99–106.

Fryer, P., Wheat, C. G., and Mottl, M. J., 1999. Mariana Blueschist mud volcanism: implications for conditions within the subduction zone, Geology, 27(2), 103-106.

Fryer, P., Wheat, C. G., Williams, T., and the Expedition 366 Scientists, 2018. Mariana Convergent Margin and South Chamorro Seamount. Proceedings of the International Ocean Discovery Program, 366: College Station, TX (International Ocean Discovery Program). https://doi.org/10.14379/iodp.proc.366.2018

King, H. M., 2020. Halite, Geology.com. https://geology.com/minerals/halite.shtml

Kohyama, N., 2007. "Quantitative analysis of each polytype of serpentine minerals and the application to industrial health and geological science." *Journal of the Clay Science Society of Japan (in Japanese)* 46(1): 33-39.

Koo, T.-H. and Kim, J., 2020. Controls on the Formation and Stability of Siderite (FeCO3) and Chukanovite (Fe2(CO3) (OH)2) in Reducing Environment, Minerals 2020, 10(2), 156.

Lavina, B., Przemyslaw Dera, and Robert T. Downs. 2014. "Modern X-ray diffraction methods in mineralogy and geosciences." *Reviews in Mineralogy and Geochemistry* 78(1): 1-31.

McNeill, L. C., Dugan, B., Petronotis, K. E., and the Expedition 362 Scientists, 2017, *Proceedings of the International Ocean Discovery Program* Volume 362 publications.iodp.org (pp. 9-10).

Meijer, A., Anthony, E. and Reagan, M., 1981. Petrology of volcanic rocks from the Forearc Sites. In Hussong, D. M., Uyeda, S., et al., Init. Repts. DSDP, 60: Washington (U.S. Govt. Printing Office), Chapter 38:709-729. (http://deepseadrilling.org/60/volume/dsdp60_38.pdf)

Natland J. H. and Tarney, J., 1981. Petrologic Evolution of the Mariana Arc and Back-Arc Basin System—A Synthesis of Drilling Results in the South Philippine Sea. in D.M. Hussong, S. Uyeda, et al., 1981, Initial Reports of the Deep-Sea Drilling Project, v. 60, U.S. Gov't Printing Office, Washington, D.C., 877-908.

Nozaka, T., Fryer, P., and Andreani, M., 2008. Formation of clay minerals and exhumation of lower-crustal rocks at Atlantis Massif, Mid-Atlantic Ridge, Geochem. Geophys. Geosyst., 9, Q11005, doi:10.1029/2008GC002207.

Ohara Y, Reagan MK, Fujikura K, Watanabe H, Michibayashi K, Ishii T, Stern RJ, Pujana I, Martinez F, Girard G, Ribeiro J, Brounce M, Komori N, Kino M. 2011. A serpentinite-hosted ecosystem in the Southern Mariana Forearc. Proc Natl Acad Sci USA 109(8):2831-2835.

Reagan, M. K., Mohler, D. Brian, H., Hickey-Vargas, R., Hanan, B., 2003. American Geophysical Union, Fall Meeting 2003, abstract id. T31A-02. 2003AGUFM.T31A..02R (https://ui.adsabs.harvard.edu/abs/2003AGUFM.T31A.02R/abstract)

Saboda, K. L., Fryer, P., Maekawa, H., 1992. Metamorphism of ultramafic clasts from Conical Seamount: Leg 125 Sites 778,779, 780, in Ocean Drilling Program Leg 125, Scientific Results Leg 125, 431-443.

Wood, D. A., Marsh, N. G., Tarney, J., Joron, J. L., Fryer, P., and Treuil, M., 1981. Geochemistry of igneous rocks recovered from a transect across the Mariana Trough, Arc, Forearc and Trench, sites 453 to 461, DSDP Leg 60, in D.M. Hussong, S. Uyeda, et al., 1981, Initial Reports of the Deep Sea Drilling Project, v. 60, U.S. Gov't Printing Office, Washington, D.C., 611-646.